On the tension-compression switch of the Gasser–Ogden–Holzapfel model: Analysis and a new pre-integrated proposal.

Marcos Latorre, Francisco J. Montáns

Universidad Politécnica de Madrid. Escuela Técnica Superior de Ingeniería Aeronáutica y del Espacio. Plaza Cardenal Cisneros 3, 28040 Madrid, Spain.

m.latorre.ferrus@upm.es; fco.montans@upm.es.

Abstract

Many biological soft tissues are structurally composed of a mostly isotropic matrix (elastin) and fibers (collagen) disposed in preferred directions which depend on the structural mission of the tissue. These fibers are not perfectly aligned but their orientation is statistically dispersed around some referential directions. The matrix is usually modelled as an isotropic, isochoric, hyperelastic material, whereas the fibers are frequently modelled employing exponential Fung-type functions of anisotropic invariants. In order to account for the dispersion of the fibers, a probability distribution is assumed. The Generalized Structure Tensor (GST) models perform a pre-integration of the distribution in order to achieve improved computational efficiency. The best known model of this kind is the Gasser-Ogden-Holzapfel (GOH) model. However, in these models no singular treatment of fibers is made. Whenever they suffer compression it is usual to consider that fibers should not contribute to the overall stiffness. At this point, a switch criterion is employed. This switch criterion is important because it changes the model predictions and may also result in unphysical stress predictions or strain ranges at which no compatible equilibrium solution is found. We perform an analysis of different tension-compression switch criteria from the literature for the GOH model and show relevant physical and computational drawbacks when using these criteria. In order to overcome these drawbacks, we make a new proposal which yield continuous stress solutions. In our proposal, pre-integrated expressions given in terms of the usual set of invariants take into account an average amount of fibers working either in tension or in compression for a given deformation gradient and fiber family. Two distinct switch criteria naturally emerge from our procedure. Furthermore, we keep the appealing GST pre-integrated approach for any proposed stored energy for the fibers, including that of the GOH model.

Keywords: Anisotropy, Generalized Structure Tensor, biological tissues, fiber dispersion, arterial wall mechanics, collagen.

1 Introduction

Soft biological tissues are usually modelled as hyperelastic materials [1], [2]. Because of the high water content, they are typically regarded as quasi-incompressible materials [1]. Frequently, these materials may be considered composed of an isotropic soft matrix (mostly elastin) and of stiffer fibers (collagen) [3] in a layout disposed by nature depending on their structural task. These fibers are distributed in a disperse manner about some preferred directions [4]. The distribution and

dispersion of the fibers as well as the orientation of these directions themselves largely depend on the specific tissue and even on the specific location of that tissue in the body, see for example [5], [6], [7], [8], [9] among others.

There are several possible approaches to model these materials. One possible approach is to address the problem in a purely phenomenological way. In this case, no information is employed about fiber existence or distribution in the material. The material is treated as a whole. We presented two models based on this approach for transversely isotropic and orthotropic materials in References [10] and [11], respectively. In contrast with many typical anisotropic hyperelastic models, these formulations use logarithmic strains and the associated invariants as a natural extension of the infinitesimal ones [12], [13], [14] in such a way that the corresponding infinitesimal model is recovered for small strains, a desirable feature for hyperelastic large strain models [15], along with that of material-symmetries congruency [16]. Furthermore, the number of experimental curves employed to determine these models are the same as the number of constants that define the infinitesimal behavior, a feature that allows to capture the transverse deformation effects in arterial wall specimens [17]. These models are mainly computational (i.e. no analytical expression is assumed for the stored energy) and are formulated following the spline-based approach firstly introduced in [18] for isotropic materials, i.e. they exactly capture the prescribed behavior. This framework can be extended to include the Mullins effect [19] and also to capture the instantaneous and relaxed behavior in viscous anisotropic materials [20], [21]. Since no fiber information is employed, no tension-compression distinction for fibers is needed: all the information is already assumed to be included in the macroscopic experimental stress-strain behavior, which is exactly captured without the need of any parameter-fitting procedure [17].

Another approach is to use the information about the substructure of the material, i.e. the fiber orientation and the angular distribution, and separate the nonlinear behavior of both matrix and fibers. With these models, the influence of variations on the fiber content, orientation and distribution may be explicitly considered, so they are particularly interesting from theoretical and micromechanical perspectives. Also explicit analytical functions of the stored energy of the constituents are assumed and usually written in terms of anisotropic invariants of the Cauchy–Green deformation tensor [22], [23]. The composite stored energy function is assumed to be the addition of the (distinct) energy functions of the constituents.

In these models, the fiber distribution is integrated to yield the stresses which are added to those in the matrix. One of the first models of this kind is that of Lanir [24], [25]. Here two main types of models may be distinguished. In the first type of models, frequently named Angular Integration (AI) models, fibers are considered separately and the integration of the distribution is performed during the analysis at each stress integration point for the specific deformation at hand. Therefore, the computational cost may be important. Examples of these models which use different probability density functions (von Mises, Gaussian, etc.) and dispersion patterns are given in Refs [26], [27], [28] and [29], among others. See review of contributions in [30].

The second type of microstructurally-based models are computationally more economical for finite element analysis. In these models the fiber distributions are pre-integrated and the result is somehow encapsulated in Generalized Structure Tensors (GST). Examples are those of References [31], [4], [32], see also analysis in [33]. These tensors contain material parameters which include the information of the mean of the distribution and sometimes higher order moments, as in the GHOST (Generalized High Order Structure Tensor) [34] and Pandolfi-Vasta models [32]. This family of models is very important from a computational point of view because it allows for the inclusion of microstructure information without a relevant penalty from a computational point of

view. One of the first models of this kind is the model of Gasser, Ogden and Holzapfel (GOH) [4]. In particular, this model is being extensively used in biomechanics and is now available in commercial finite element codes, as in Abaqus [36]. The simpler precursor model in Ref. [3] is also available in Adina [37]. Clearly, the model in Ref. [4] represents an improvement to that detailed in Ref. [3], which has been considered one of the best contributions in the field in the last twenty years [35].

However, one of the controversial issues of the GOH model is how to account for the fiber distribution stiffness when the stretch in the main fiber direction is less (or equal) than one, a relevant and nonstraightforward problem [30]. The inconvenience of the use of the GST approach when compared to the AI one, in particular as presented by Gasser et al [4], is that since all fibers are treated as a whole, it is not possible to distinguish different fiber contributions when some of them are in tension (and hence contribute to the global stiffness) and some in compression (and their stiffness contributions are neglected). This is an issue relevant even for isotropic distributions of fibers [33], [34]. This singularity is handled through a tension-compression switch criterion which determines both the point at which the relevant anisotropic part of the fiber family stiffness is no longer considered and how the vanishing of the stiffness is taken into account. The original proposal of Gasser et al. has been found to be inadequate [33] and has been modified in the implementation in Abaqus [36], where a different switch based on an averaged structure invariant is used. This latter implementation has been criticized recently by Holzapfel and Ogden [38], who considered that the switch criterion should be given by the fourth structural invariant. In this recent work [38], Holzapfel and Ogden give a proposal for the cases when fibers work in compression which somehow goes back to the ideas of Lanir [24], [25] and which, for a general stored energy for the fibers, requires the numerical integration of the fiber distributions at the stress integration points during finite element simulations. Furthermore, it requires the solution of a nonlinear equation to determine the critical angles which deppend on the components of the Green-Cauchy deformation tensor at the given stress integration point.

From the previous lines, it is obvious that there is an important controversy regarding the proper switch for the GOH model [4] and that there is a need for an efficient, pre-integrated approach which give continuous stress functions and which keeps the essence of the GST models in general and the GOH model in particular. In this work we first analyze the different proposals in the literature and show some drawbacks in those proposals. In order to solve the detected problems, we propose a new alternative. In our approach we properly account for the *average* amount of fibers working in tension and those working in compression, determining the angle at which fibers remain unstretched in average. However, we still keep the GST philosophy: fiber distributions are still pre-integrated through a modified, weighted, structure invariant, regardless of the stored energy function employed for the fibers. Two distinct physically-motivated, invariant-based switch criteria naturally emerge from our procedure.

The layout of the remaining part of the paper is as follows. We first summarize the GOH model without switch and particularize for uniaxial testing with fibers working in tension and compression. Then we analyze the switch proposals by Gasser et al [4] and by Abaqus [36], highlighting the difficulties encountered. We finally explain and analyze our proposal and show that the predicted stresses are consistent and continuous for all strain ranges. We also remark the differences of the present proposal with the recent one given by Holzapfel and Ogden in Reference [38].

2 The fiber dispersion model of Gasser et al. [4]

In this work we study the mechanical behavior of arterial wall specimens under uniaxial testing using the well-known GST model of Gasser et al. [4]. We perform a parametric analysis for different distributed orientations of the collagen fiber bundles in the soft tissue considering different hypothesis for the compression response of the fibers, leading to remarkably different results. It will be assumed (throughout this work) that the arterial wall deformation is purely isochoric.

The GOH-GST hyperelastic model is formulated in Ref. [4] by means of an isochoric strain energy function $\mathcal{W}$ including two main contributions. The first contribution, $\mathcal{W}_g$, accounts for the purely isotropic behavior of the ground substance, whereas the second one, $\mathcal{W}_f$, accounts for the anisotropic contribution associated with the fibers within the tissue. Specifically, $\mathcal{W}_f = \sum_{i=1}^{2} \mathcal{W}_{fi}$ describes the behavior of two families of fibers separately, each family being characterized by a distribution of fibers arranged with rotational symmetry about its corresponding referential direction $\boldsymbol{a}_{0i}$. The strain energy function $\mathcal{W}_g$ is formulated in Ref. [4] in terms of the first principal invariant of the right Cauchy–Green isochoric deformation tensor $\bar{\boldsymbol{C}}$, namely $\bar{I}_1 = \operatorname{tr} \bar{\boldsymbol{C}} = \boldsymbol{I} : \bar{\boldsymbol{C}}$, by means of the incompressible neo-Hookean model $\mathcal{W}_g(\bar{I}_1) = \frac{1}{2} c(\bar{I}_1 - 3)$, where c is the neo-Hookean parameter. Each transversely isotropic free-energy function $\mathcal{W}_{fi}$ is represented by the (same) single-variable Fung-type exponential function

$$\mathcal{W}_{fi}(\bar{E}_i) = \mathcal{W}_f(\bar{E}_i) = \frac{k_1}{2k_2} \left[\exp\left(k_2 \bar{E}_i^2\right) - 1 \right] \tag{1}$$

which directly depends on the so-called structure invariant $\bar{E}_i$ relative to the ith fiber family (k_1 and k_2 are material parameters). The structure invariant $\bar{E}_i$ represents an averaged (or weighted) Green–Lagrange strain measure associated with the ith dispersed fiber family defined through [30]

$$\bar{E}_i = \boldsymbol{H}_i : (\bar{\boldsymbol{C}} - \boldsymbol{I}) = \boldsymbol{H}_i : \bar{\boldsymbol{C}} - \operatorname{tr} \boldsymbol{H}_i \tag{2}$$

where

$$\boldsymbol{H}_i = \kappa \boldsymbol{I} + (1 - 3\kappa)\, \boldsymbol{a}_{0i} \otimes \boldsymbol{a}_{0i} \tag{3}$$

is a Generalized Structure Tensor that characterizes, and quantifies, the fiber dispersion effects about the main orientation $\boldsymbol{a}_{0i}$ through an additional (structure) material parameter κ. This formulation is justified by a truncated series expansion of the AI model [32], [33]. Other structure-tensor-based approaches, which take into account higher-order terms in the Taylor expansion, can be seen in Refs. [32], [34].

For the GST model, Eq. $(2)_2$ reads

$$\begin{aligned}
\bar{E}_i &= [\kappa \boldsymbol{I} + (1 - 3\kappa)\, \boldsymbol{a}_{0i} \otimes \boldsymbol{a}_{0i}] : \bar{\boldsymbol{C}} - \operatorname{tr} [\kappa \boldsymbol{I} + (1 - 3\kappa)\, \boldsymbol{a}_{0i} \otimes \boldsymbol{a}_{0i}] && (4)\\
&= \left[(\kappa \boldsymbol{I}) : \bar{\boldsymbol{C}} - \operatorname{tr} (\kappa \boldsymbol{I}) \right] + \left[((1 - 3\kappa)\, \boldsymbol{a}_{0i} \otimes \boldsymbol{a}_{0i}) : \bar{\boldsymbol{C}} - \operatorname{tr} ((1 - 3\kappa)\, \boldsymbol{a}_{0i} \otimes \boldsymbol{a}_{0i}) \right] && (5)\\
&= \kappa(\bar{I}_1 - 3) + (1 - 3\kappa)\, (\bar{I}_{4i} - 1) && (6)
\end{aligned}$$

where the pseudo-invariant $\bar{I}_{4i} := \boldsymbol{a}_{0i} \otimes \boldsymbol{a}_{0i} : \bar{\boldsymbol{C}}$ represents the squared stretch of the fiber oriented about the referential direction $\boldsymbol{a}_{0i}$. In Ref. [4], the value of the dispersion parameter was shown to be within the range $\kappa \in [0, 1/3]$. For $\kappa = 0$ it is obtained $\boldsymbol{H}_i \equiv \boldsymbol{a}_{0i} \otimes \boldsymbol{a}_{0i}$ and $\bar{E}_i \equiv \bar{I}_{4i} - 1$, so the anisotropic contributions reduce to those of the model with perfectly aligned fibers described in Ref. [3], i.e. $\mathcal{W}_f(\bar{E}_i) \equiv \mathcal{W}_f(\bar{I}_{4i} - 1)$. The value $\kappa = 1/3$ is associated with the case with isotropically distributed fibers, for which $\boldsymbol{H}_i \equiv \frac{1}{3}\boldsymbol{I}$ and $\bar{E}_i \equiv \bar{I}_1/3 - 1$, so each contribution $\mathcal{W}_f(\bar{E}_i) \equiv$

$\mathcal{W}_f(\bar{I}_1/3-1)$ becomes isotropic in the limit, i.e. there is no preferred orientation of the fibers within each family. As pointed out in Ref. [39], the absolute upper limit on κ may be $\frac{1}{2}$. If compressed fibers are not appropriately treated, both ranges $\kappa \in [0, 1/3]$ and $\kappa \in (1/3, 1/2]$ can lead to unphysical results, the first range for compression along the main fiber direction and the second one for extension along the main fiber direction [33]. For further use, the modified second Piola–Kirchhoff stresses $\bar{\boldsymbol{S}} = 2d\mathcal{W}/d\bar{\boldsymbol{C}}$ that directly derive from the total strain energy function $\mathcal{W} = \mathcal{W}_g + \sum_{i=1}^{2} \mathcal{W}_{fi}$ are

$$\bar{\boldsymbol{S}} = 2\frac{d\mathcal{W}_g}{d\bar{I}_1}\frac{d\bar{I}_1}{d\bar{\boldsymbol{C}}} + \sum_{i=1}^{2} 2\frac{d\mathcal{W}_f}{d\bar{E}_i}\frac{d\bar{E}_i}{d\bar{\boldsymbol{C}}} \tag{7}$$

$$= c\boldsymbol{I} + \sum_{i=1}^{2} 2\mathcal{W}_f'(\bar{E}_i)\boldsymbol{H}_i \tag{8}$$

where $\mathcal{W}_f'(\bar{E}_i)$ is the first derivative function of the strain energy function of Eq. (1)

$$\mathcal{W}_f'(\bar{E}_i) = k_1 \bar{E}_i \exp\left(k_2 \bar{E}_i^2\right) \tag{9}$$

Uniaxial testing

In order to analyze the difficulties encountered when fibers work in compression in a specific problem, we present some numerical results from uniaxial tensile tests performed over arterial wall specimens using the preceding *GST* model. The material parameters $c = 7.64\,\text{kPa}$, $k_1 = 996.6\,\text{kPa}$ and $k_2 = 524.6$ are taken from Ref. [4]. The angle $\gamma = 49.98^o$, that defines the main orientation of both fiber families within the arterial layer ($\boldsymbol{a}_{01} = [\cos\gamma, -\sin\gamma, 0]$, $\boldsymbol{a}_{02} = [\cos\gamma, \sin\gamma, 0]$), is also taken from that Reference, see Figure 1. For the circumferential specimen the uniaxial tensile test is performed along axis 1 (with the stretch $\lambda_1 \geq 1$) and the corresponding uniaxial tensile test for the axial strip is performed along axis 2 (for which $\lambda_2 \geq 1$). The modified second Piola–Kirchhoff stresses $\bar{\boldsymbol{S}}$ of Eq. (8) in this case specialize to

$$\bar{\boldsymbol{S}} = \left[c + 4\mathcal{W}_f'(\bar{E})\kappa\right]\boldsymbol{I} + 4\mathcal{W}_f'(\bar{E})\,(1-3\kappa)\,\boldsymbol{A}_0 \tag{10}$$

where $\boldsymbol{A}_0 := \frac{1}{2}\sum_{i=1}^{2} \boldsymbol{a}_{0i} \otimes \boldsymbol{a}_{0i}$. The invariants $\bar{E} := \bar{E}_1 = \bar{E}_2$, $\bar{I}_1$ and $\bar{I}_4 := \bar{I}_{41} = \bar{I}_{42}$ are given by

$$\bar{E} = \kappa(\bar{I}_1 - 3) + (1-3\kappa)\,(\bar{I}_4 - 1) \tag{11}$$

$$\bar{I}_1 = \lambda_1^2 + \lambda_2^2 + 1/(\lambda_1^2\lambda_2^2) \tag{12}$$

$$\bar{I}_4 = \lambda_1^2\cos^2\gamma + \lambda_2^2\sin^2\gamma \tag{13}$$

where the incompressibility constraint $\lambda_1\lambda_2\lambda_3 = 1$ has been used in the expression of $\bar{I}_1$. The only non-vanishing components of the second-order tensor $\boldsymbol{A}_0$ in Eq. (10), expressed in the reference frame $X_{123} = \{1, 2, 3\}$ of Figure 1, are $(A_0)_{11} = \cos^2\gamma$ and $(A_0)_{22} = \sin^2\gamma$. The corresponding Kirchhoff stresses $\bar{\boldsymbol{\tau}} = \bar{\boldsymbol{X}}\bar{\boldsymbol{S}}\bar{\boldsymbol{X}}^T$ are readily obtained from the second Piola–Kirchhoff stresses $\bar{\boldsymbol{S}}$ of Eq. (10) and the isochoric deformation gradient tensor $\bar{\boldsymbol{X}} = diag\,[\lambda_1, \lambda_2, 1/(\lambda_1\lambda_2)]$. Since the deformation is purely isochoric, $J = \det\boldsymbol{X} = \det\bar{\boldsymbol{X}} = 1$, the associated Cauchy stress tensor is $\bar{\boldsymbol{\sigma}} = \bar{\boldsymbol{\tau}}$. Finally, the total Cauchy stresses are given by $\boldsymbol{\sigma} = \bar{\boldsymbol{\sigma}} + p\boldsymbol{I}$, where p is an additional hydrostatic pressure to be obtained from the equilibrium equations of the uniaxial tests and the

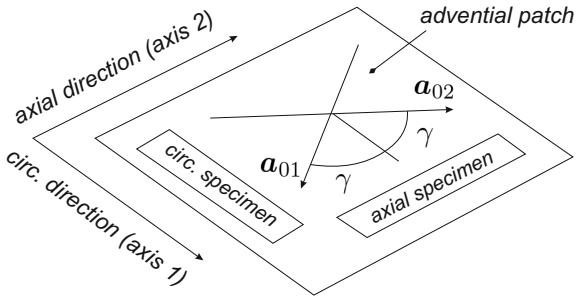

Figure 1: Definition of circumferential and axial specimens for the tensile tests. $\gamma = 49.98^o$.

consideration of the respective boundary conditions. We note that the stress tensor $\bar{\boldsymbol{\sigma}}$ may contain a hydrostatic contribution because we have not projected it to the deviatoric space using the proper fourth-order projection tensor. However, this operation is irrelevant in the present purely incompressible case because this projection would only change the specific numerical value of p obtained from the equilibrium equations at each deformation state. In the next sections, we provide the solution to the equilibrium equations of both uniaxial tests when different treatments of the compressive behavior of fibers are considered in the model.

For further comparison among the different tension-compression switch criteria analyzed in the next sections, we substitute Eq. (6) into Eq. (1) and represent in Figure 2 the strain energy function associated with the ith fiber family as a function of the invariants $\bar{I}_1$ and $\bar{I}_{4i}$, i.e. $\mathcal{W}_f(\bar{E}_i) = \mathcal{W}_f(\bar{I}_1, \bar{I}_{4i})$, for the particular case $\kappa = 0.226$ (taken also from Ref. [4]). We will see that each proposed switch modifies the anisotropic *compressive* part of this function in a different way, hence leading to remarkably different results.

3 Model with fibers working in tension *and* compression

We now consider the unmodified model in which fibers are working both in tension and compression according to their also unmodified energy functions.

Uniaxial testing

For the uniaxial tensile test performed over the circumferential specimen (axis 1 in Figure 1, $\lambda_1 \geq 1$), the boundary conditions are $\sigma_2 = \sigma_3 = 0$. After eliminating the pressure from the system of equations $\boldsymbol{\sigma} = \bar{\boldsymbol{\sigma}} + p\boldsymbol{I}$, we arrive at

$$\sigma_1 = \left(c + 4\mathcal{W}_f'(\bar{E})\kappa\right)\left(\lambda_1^2 - \frac{1}{\lambda_1^2\lambda_2^2}\right) + 4\mathcal{W}_f'(\bar{E})\left(1-3\kappa\right)\lambda_1^2\cos^2\gamma \tag{14}$$

$$0 = \left(c + 4\mathcal{W}_f'(\bar{E})\kappa\right)\left(\lambda_2^2 - \frac{1}{\lambda_1^2\lambda_2^2}\right) + 4\mathcal{W}_f'(\bar{E})\left(1-3\kappa\right)\lambda_2^2\sin^2\gamma \tag{15}$$

where Eqs. (9) and (11)–(13) are to be used. Equations (14) and (15) can be solved numerically for each stretch $\lambda_1 > 1$ to give the uniaxial (circumferential) stress $\sigma_1\left(\lambda_1\right)$ and the transverse (axial)

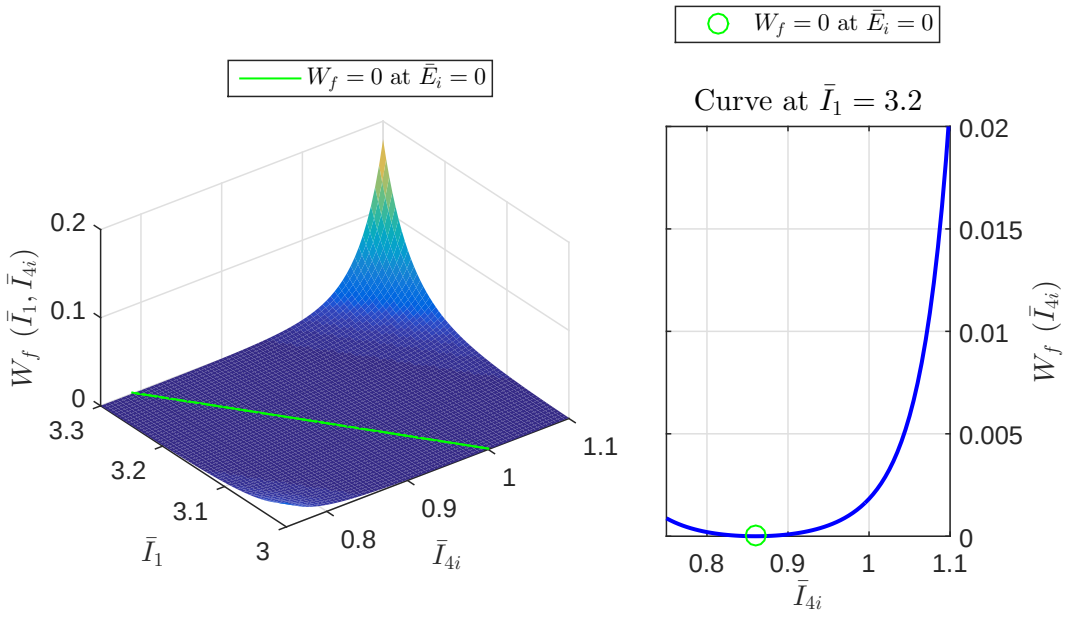

Figure 2: Original strain energy function of the ith fiber family $\mathcal{W}_f(\bar{E}_i) = \mathcal{W}_f(\bar{I}_1, \bar{I}_{4i})$ [MJ / m^3]. Equations (1) and (6) are used with $k_1 = 996.6\,\text{kPa}$, $k_2 = 524.6$ and $\kappa = 0.226$.

stretch $\lambda_2(\lambda_1)$. More specifically, we can obtain the transverse stretch $\lambda_2(\lambda_1)$ directly from Eq. (15) and then substitute in Eq. (14) to obtain the corresponding stress $\sigma_1(\lambda_1)$. The computed solution variables $\sigma_1(\lambda_1)$ and $\lambda_2(\lambda_1)$, together with the invariants $\bar{I}_4(\lambda_1)$ and $\bar{E}(\lambda_1)$ are shown in Figure 3 for the range $\lambda_1 \in [0, 1.3]$ and for different values of the dispersion parameter κ. It is important to note in Figure 3 that the invariant $\bar{I}_4$ is lower or equal than one for some values of κ within some deformation intervals which depend on the selected value of κ. Hence, we have let the fibers along the main orientations bear compression ($\bar{I}_4 < 1$) in the present analysis and we have not applied any switch criterion for fiber compression. In other words, the strain energy function of each fiber family being used in this section (for the case $\kappa = 0.226$) is that of Figure 2.

The results regarding the uniaxial test over the axial strip (axis 2 in Figure 1, $\lambda_2 \geq 1$), which boundary conditions are $\sigma_1 = \sigma_3 = 0$, are shown in Figure 4. Note that in this case the invariant $\bar{I}_4$ also reaches values lower than one for some values of the dispersion parameter κ (although $\bar{I}_4 > 1$ for the special case $\kappa = 0.226$).

4 Model with the tension-compression switch proposed by Gasser et al. [4]

If fibers do not support compressive loading at all, then some mechanism to exclude the contribution of the contracted fibers in the given potential has to be considered. The fact that the fiber dispersion is pre-integrated in GST-based approaches (which makes these models appealing from a computational standpoint) makes impossible to selectively suppress the compressed fibers within the distribution from the anisotropic strain energy function at each deformation state. In contrast, this suppression can be easily done 'fiber by fiber' in AI-based models at each location and instant, however at the cost of a much higher computational effort in generic simulations. In Reference [4] it is proposed that the anisotropic part of the generalized structure tensor $\boldsymbol{H}_i$ of Eq. (3) does not contribute to $\boldsymbol{H}_i$ when $I_{4i} = \boldsymbol{a}_{0i} \otimes \boldsymbol{a}_{0i} : \boldsymbol{C} \leq 1$ (i.e. $\bar{I}_{4i} \leq 1$ for the purely incompressible case). This is equivalent to drop the relevant part of the fiber family potential of Eq. (1), which leads to a purely isotropic response —cf. Ref. [30]. That is, if $\bar{I}_{4i} \leq 1$, the expression of the Generalized Structure Tensor of Eq. (3) reduces to

$$\boldsymbol{H}_i = \kappa \boldsymbol{I} \quad \text{if} \quad \bar{I}_{4i} \leq 1 \tag{16}$$

whereupon the structure invariant $\bar{E}_i$ reads

$$\bar{E}_i = \boldsymbol{H}_i : \bar{\boldsymbol{C}} - tr\, \boldsymbol{H}_i = \begin{cases} \kappa(\bar{I}_1 - 3) + (1 - 3\kappa)(\bar{I}_{4i} - 1) & \text{if} \quad \bar{I}_{4i} > 1 \\ \kappa(\bar{I}_1 - 3) & \text{if} \quad \bar{I}_{4i} \leq 1 \end{cases} \tag{17}$$

The general definition of the structure invariant $\bar{E}_i$ given in Eq. (2) ensures both the continuity of $\bar{E}_i(\bar{I}_1, \bar{I}_{4i})$ at $\bar{I}_{4i} = 1$ and the continuity of $\mathcal{W}_{fi}(\bar{E}_i)$ and its derivatives with respect to $\bar{E}_i$ at $\bar{E}_i(\bar{I}_1, \bar{I}_{4i} = 1) = \kappa(\bar{I}_1 - 3)$. Nevertheless, this is not sufficient to ensure continuity of stresses, in general, at the switch point $\bar{I}_{4i} = 1$ because the gradient $d\bar{E}_i/d\bar{\boldsymbol{C}} = \boldsymbol{H}_i$, present in Eqs. (7) and (8), is discontinuous at that point. This becomes apparent comparing Eq. (16) (for $\bar{I}_{4i} \leq 1$) to Eq. (3) (for $\bar{I}_{4i} > 1$) and particularizing the stress contribution of the ith dispersed fiber family given in Eq. (8) at $\bar{I}_{4i} \leq 1$ and $\bar{I}_{4i} \to 1^+$, i.e.

$$\bar{\boldsymbol{S}}_{fi}(\bar{E}_i)\big|_{\bar{I}_{4i} \leq 1} = 2\, \frac{d\mathcal{W}_f}{d\bar{E}_i} \frac{d\bar{E}_i}{d\bar{\boldsymbol{C}}}\bigg|_{\bar{I}_{4i} \leq 1} = 2\mathcal{W}_f' \left(\kappa(\bar{I}_1 - 3)\right) \kappa \boldsymbol{I} \tag{18}$$

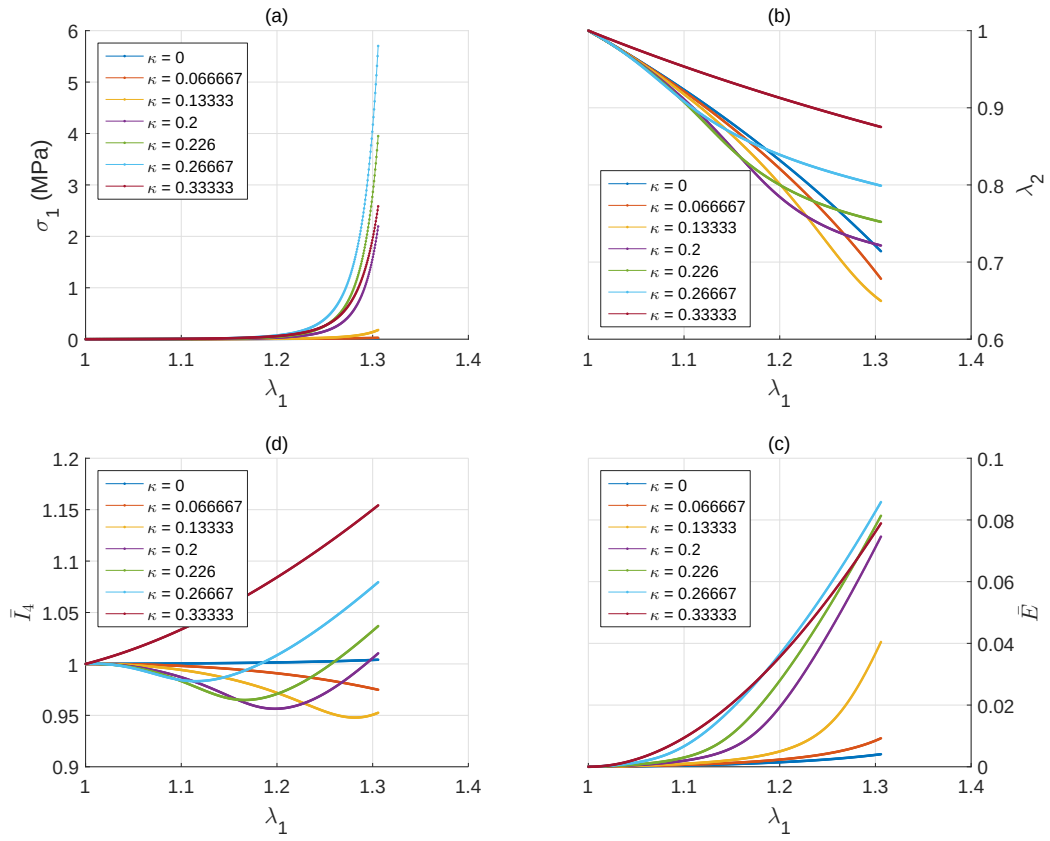

Figure 3: Uniaxial test over the circumferential specimen (direction 1 in Figure 1). Clockwise from left-up corner: (a) Uniaxial stress in circumferential direction σ_1 (b) Transverse stretch in axial direction λ_2 (c) Structure invariant $\bar{E} = \kappa(\bar{I}_1 - 3) + (1 - 3\kappa)(\bar{I}_4 - 1)$ (d) Pseudo-invariant $\bar{I}_4$: squared stretch of the fibres in the main orientations $\boldsymbol{a}_{0i}$.

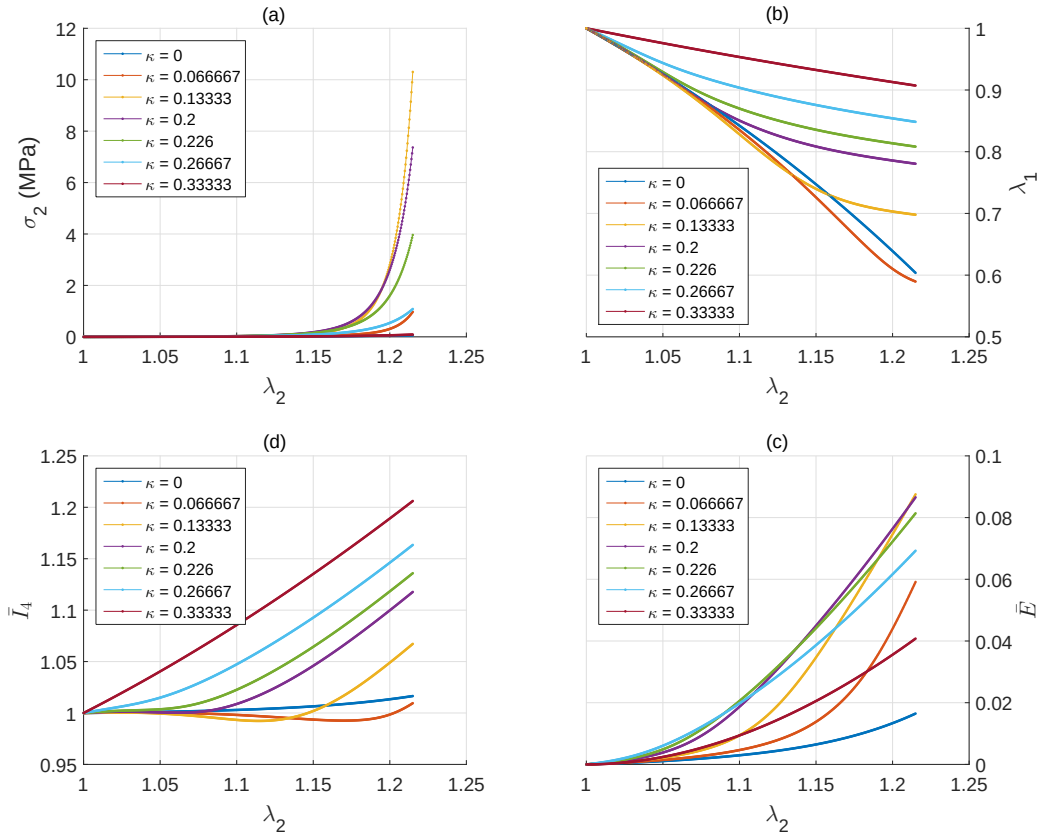

Figure 4: Uniaxial test over the axial specimen (direction 2 in Figure 1). Clockwise from left-up corner: (a) Uniaxial stress in axial direction σ_2 (b) Transverse stretch in circumferential direction λ_1 (c) Structure invariant $\bar{E} = \kappa(\bar{I}_1 - 3) + (1 - 3\kappa)(\bar{I}_4 - 1)$ (d) Pseudo-invariant $\bar{I}_4$: squared stretch of the fibres in the main orientations $\boldsymbol{a}_{0i}$.

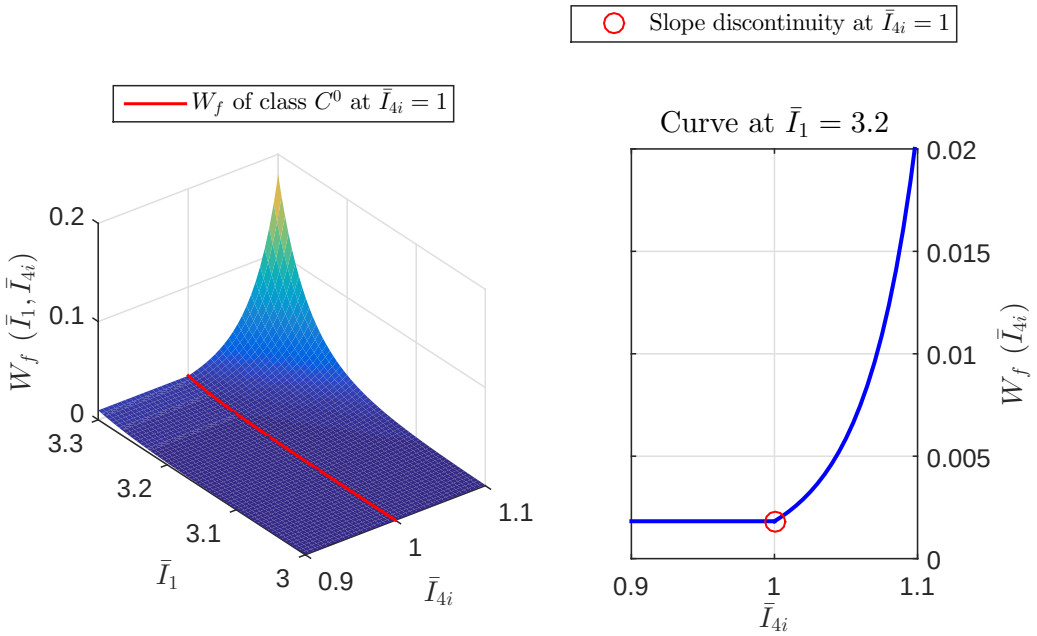

Figure 5: Strain energy function of the ith fiber family $\mathcal{W}_f(\bar{E}_i) = \mathcal{W}_f(\bar{I}_1, \bar{I}_{4i})$ [MJ / m^3] modified according to the switch $\bar{I}_{4i} \leq 1$ proposed in Ref. [4]. Equations (1) and (17) are used with $k_1 = 996.6\,\text{kPa}$, $k_2 = 524.6$ and $\kappa = 0.226$.

but

$$\bar{\boldsymbol{S}}_{fi}(\bar{E}_i)\big|_{\bar{I}_{4i}\to 1^+} = 2\,\frac{d\mathcal{W}_f}{d\bar{E}_i}\frac{d\bar{E}_i}{d\bar{\boldsymbol{C}}}\bigg|_{\bar{I}_{4i}\to 1^+} = 2\mathcal{W}_f'\left(\kappa(\bar{I}_1 - 3)\right)\left(\kappa\boldsymbol{I} + (1-3\kappa)\,\boldsymbol{a}_{0i}\otimes\boldsymbol{a}_{0i}\right) \tag{19}$$

The (modified) fiber family strain energy function $\mathcal{W}_f(\bar{E}_i)$ from which the stresses given in Eqs. (18) and (19) derive is represented in Figure 5 for $\kappa = 0.226$ as a function of the two variables $\mathcal{W}_f(\bar{I}_1, \bar{I}_{4i})$. The origin of the discontinuity of stresses at the points $(\bar{I}_1, \bar{I}_{4i} = 1)$ can be observed in that three-dimensional surface, which is a continuous function of class C^0 at those points.

Remark The strain energy function of the ith fiber family given by Eq. (1) along with Eq. (17) contains an implicit non-linear coupling between the isotropic and anisotropic parts of the structure (weighted) invariant $\bar{E}_i = \kappa(\bar{I}_1 - 3) + (1-3\kappa)\,(\bar{I}_{4i} - 1) =: \bar{E}_i^{iso} + \bar{E}_i^{ani}$. This coupling in $\mathcal{W}_f$ originates the stress discontinuities that have been observed in this section. If one wants to suppress the anisotropic part of the invariant $\bar{E}_i$ when $\bar{I}_{4i} \leq 1$ and still obtain a continuous stress response at the switch point $\bar{I}_{4i} = 1$, then a straightforward modification of the present GST model,

that follows the idea of Ref. [16], consists of decoupling the isotropic and anisotropic contributions to $\bar{E}_i$ in the strain energy function associated with the fiber family as

$$\mathcal{W}_f(\bar{E}_i^{iso}, \bar{E}_i^{ani}) = \mathcal{W}_f^{iso}(\bar{E}_i^{iso}) + \mathcal{W}_f^{ani}(\bar{E}_i^{ani}) \tag{20}$$

where $\bar{E}_i^{iso} = \bar{E}^{iso} = \kappa(\bar{I}_1 - 3)$ and $\bar{E}_i^{ani} = (1-3\kappa)\,(\bar{I}_{4i} - 1)$. Different strain energy functions may be used for the isotropic and anisotropic contributions in Eq. (20), thereby the dependence on $\bar{E}^{iso}$ and $\bar{E}_i^{ani}$ may be fitted to the specific material behavior. Note that the isotropic contribution $\mathcal{W}_f^{iso}(\bar{E}_i^{iso})$ depends on the isotropic behavior of the fiber family distribution, which is different to the matrix constituent behavior accounted for by the energy component $\mathcal{W}_g$. The fiber family strain energy function of Eq. (20) may be formulated in order to satisfy continuity of slopes (partial derivatives) over the points $(\bar{I}_1, \bar{I}_{4i} = 1)$. Assume for simplicity that both $\mathcal{W}_f^{iso}$ and $\mathcal{W}_f^{ani}$ are given by the same exponential function of Eq. (1). The next switch criterion *naturally* follows for the modified second Piola–Kirchhoff stress tensor $\bar{\boldsymbol{S}}_{fi} = 2d\mathcal{W}_f(\bar{E}^{iso})/d\bar{\boldsymbol{C}} + 2d\mathcal{W}_f(\bar{E}_i^{ani})/d\bar{\boldsymbol{C}}$

$$\bar{\boldsymbol{S}}_{fi}(\bar{E}^{iso}, \bar{E}_i^{ani} > 0) = 2\mathcal{W}_f'(\bar{E}^{iso})\kappa\boldsymbol{I} + 2\mathcal{W}_f'(\bar{E}_i^{ani})\,(1-3\kappa)\,\boldsymbol{a}_{0i} \otimes \boldsymbol{a}_{0i} \tag{21}$$

$$\bar{\boldsymbol{S}}_{fi}(\bar{E}^{iso}, \bar{E}_i^{ani} \leq 0) = 2\mathcal{W}_f'(\bar{E}^{iso})\kappa\boldsymbol{I} \tag{22}$$

This criterion yields continuous stresses at $\bar{I}_{4i} = 1$ due to the fact that the isotropic and anisotropic responses are uncoupled and also because $\bar{\boldsymbol{S}}_{fi}^{ani} = 2\mathcal{W}_f'(\bar{E}_i^{ani})\,(1-3\kappa)\,\boldsymbol{a}_{0i} \otimes \boldsymbol{a}_{0i}$ approaches to $\boldsymbol{0}$ in the limit $\bar{I}_{4i} \to 1^+$ (i.e. $\bar{E}_i^{ani} \to 0^+$). The hyperelastic response for $\bar{I}_{4i} \leq 1$ is purely isotropic and coincident to the one proposed by Gasser et al. [4], compare Eq. (18) to Eq. (22). Moreover, the model of Ref. [3], Eq. (26) below, is recovered for $\kappa = 0$ because $\bar{E}^{iso} \equiv 0$ and $\bar{E}_i^{ani} \equiv (\bar{I}_{4i} - 1)$. A more elaborated, physically-based solution is explained below in Section 6.

Uniaxial testing

In Section 3 we have computed some deformation intervals for which $\bar{I}_{41} = \bar{I}_{42} = \bar{I}_4 \leq 1$ in the uniaxial test over the circumferential direction, see Figure 3.*d*. Hence, the computed results are not the solution for those values of the dispersion parameter κ within their respective ranges of λ_1 for which $\bar{I}_4 \leq 1$.

From now on we analyze the case $\kappa = 0.226$ only, for which $\bar{I}_4 \leq 1$ within the interval $1.0132 \lessapprox \lambda_1 \lessapprox 1.256$. Using Eqs. (16) and $(17)_2$, the total stress response of Eq. (10) lacks the anisotropic contribution

$$\bar{\boldsymbol{S}} = \left[c + 4\mathcal{W}_f'\left(\kappa(\bar{I}_1 - 3)\right)\kappa\right]\boldsymbol{I} \tag{23}$$

so the (hyperelastic) response becomes isotropic. The transverse stretches are directly known in these cases for each λ_1 from the incompressibility constraint, i.e. $\lambda_2 = \lambda_3 = \lambda_1^{-1/2}$ (the same result is obtained from Eq. (15) with the second addend in the right-hand side removed). The equilibrium Equation (14) reduces then to

$$\sigma_1 = \left[c + 4\mathcal{W}_f'\left(\kappa(\bar{I}_1 - 3)\right)\kappa\right]\frac{\lambda_1^3 - 1}{\lambda_1} \tag{24}$$

with $\bar{I}_1 = (\lambda_1^3 + 2)/\lambda_1$, which would give the uniaxial Cauchy stresses associated with the new deformation states. However, in this case, we observe in Figure 6 that the invariant $\bar{I}_4$ (squared stretch of the referential fiber orientations) becomes greater than one for purely isotropic responses and also that it is discontinuous at the switch points due to the abrupt change from anisotropic

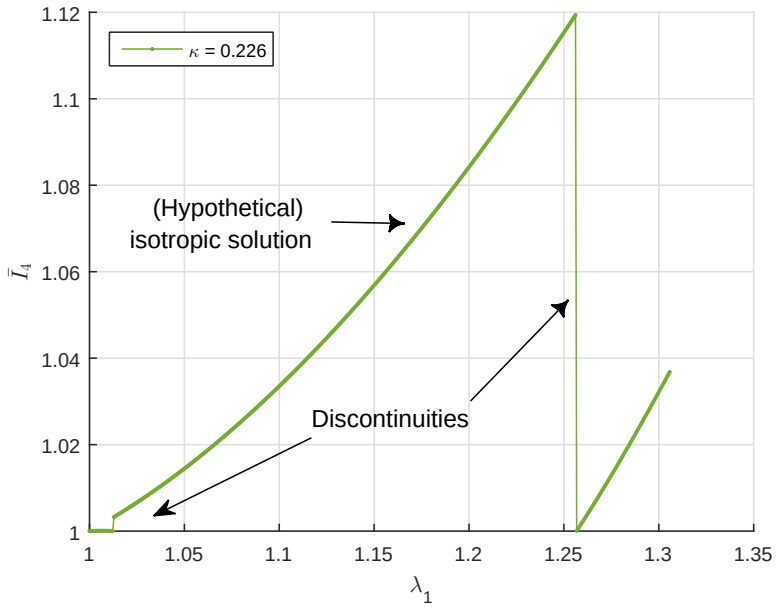

Figure 6: Uniaxial test over the circumferential specimen (direction 1 in Figure 1). Pseudo-invariant $\bar{I}_4$: squared stretch of the fibres in the main orientations $\boldsymbol{a}_{0i}$. Results using the (discontinuous) tension-compression switch of Gasser et al. [4].

to isotropic material behavior (the uniaxial stress σ_1 is also discontinuous at both points). Hence, note that we have just arrived to a contradiction within this interval, because the response should be isotropic if Eqs. (16)-(18) are employed (due to the fact that the fibers were in contraction), but the main fiber orientations are in extension if the response is isotropic. Thus, we interpret this result as that no equilibrium solution is found for this value of κ within the interval of λ_1 for which $\bar{I}_4 \leq 1$ in Section 3, i.e. $1.0132 \lessapprox \lambda_1 \lessapprox 1.256$. Note that the conclusion at which we have arrived is physically meaningless because, obviously, we should be able to stretch the circumferential specimen of this hyperelastic material within the critical interval under study and reach the corresponding equilibrium states. The interval for which no solution is found in the circumferential uniaxial test with this model is shown in Figure 7 for the case $\kappa = 0.226$. Similar situations can be encountered for other values of the material parameters if this (discontinuous) mechanism of compressed fiber exclusion is considered for this model.

We may interpret the results shown in Figures 6 and 7 in another way. If, for a given uniaxial stretch $\lambda_1 > 1$, the solution with fibers being included gives $\bar{I}_4 < 1$ (i.e. fibers should not be working) and the solution with fibers being excluded gives $\bar{I}_4 > 1$ (i.e. fibers should be resisting load), then the main fiber orientations should deform in such a way that $\bar{I}_4 = 1$. In that case, the transverse stretch λ_2 that is compatible with $\bar{I}_4 = 1$ is given from Eq. (13)

$$\left(\lambda_2^2\right)_{comp} = \frac{1 - \lambda_1^2 \cos^2\gamma}{\sin^2\gamma} \tag{25}$$

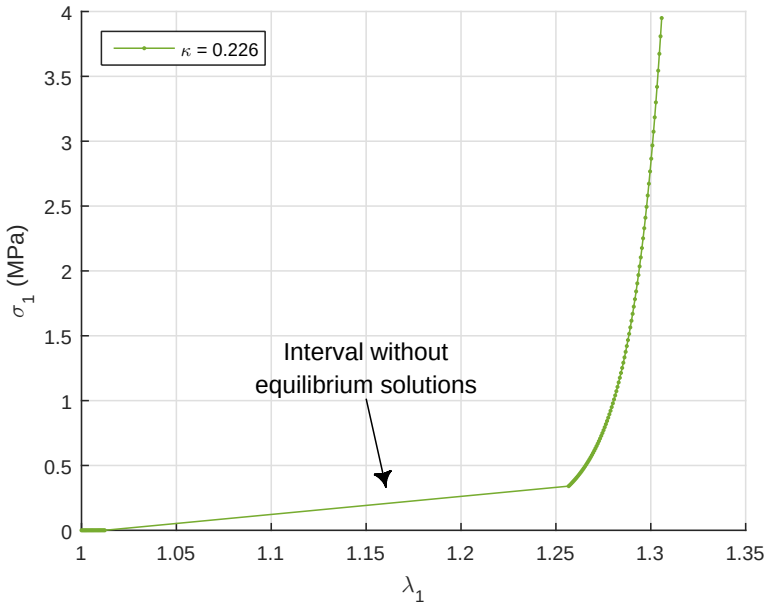

Figure 7: Uniaxial test over the circumferential specimen (direction 1 in Figure 1). Uniaxial stresses σ_1 corresponding to the (discontinuous) tension-compression switch of Gasser et al. [4]. No equilibrium solutions are possible at $1.0132 \lessapprox \lambda_1 \lessapprox 1.256$. Within that interval, if the response is assumed anisotropic, then $\bar{I}_4 < 1$, see Figure 3.*d*; on the other hand, if the response is assumed isotropic, then $\bar{I}_4 > 1$, see Figure 6.

However, it is readily verified that the transverse equilibrium condition given by Eq. (15), with $\bar{I}_4 = 1$ and the second addend in the right-hand side removed, is not satisfied for the values $(\lambda_2^2)_{comp}$. Indeed, the fulfillment of the transverse (stress-free) condition gives the isotropic solution $(\lambda_2^2)_{equil} = 1/\lambda_1$. In other words, we cannot ensure in general that both compatibility and equilibrium equations are simultaneously satisfied if the present switch for $\bar{I}_4 \leq 1$ is used for the present GST model.

Note that a simple way of preventing these discontinuities is to use the uncoupled model of Eq. (20), which provides a continuous behavior for stresses and deformations when the switch $\bar{I}_4 \leq 1$ is reached. Therefore, equilibrium solutions are always obtained.

5 Model with the tension-compression switch implemented in Abaqus [36]

For the case of perfectly aligned fibers, i.e. $\kappa = 0$, the tension-compression switching criterion is straightforward. The strain energy function for the ith (aligned) fiber family of Eq. (1) reduces in that case to

$$\mathcal{W}_f(\bar{I}_{4i} - 1) = \frac{k_1}{2k_2}\left[\exp\left(k_2(\bar{I}_{4i} - 1)^2\right) - 1\right] \tag{26}$$

and their associated modified second Piola–Kirchhoff stresses

$$\bar{\boldsymbol{S}}_{fi}(\bar{I}_{4i}) = 2k_1(\bar{I}_{4i} - 1)\exp\left(k_2(\bar{I}_{4i} - 1)^2\right)\boldsymbol{a}_{0i} \otimes \boldsymbol{a}_{0i} = 2\mathcal{W}_f'\left(\bar{I}_{4i} - 1\right)\boldsymbol{a}_{0i} \otimes \boldsymbol{a}_{0i} \tag{27}$$

Hence, in this case, we can define a (continuous) piecewise function of the invariant $\bar{I}_{4i}$ as

$$\bar{I}_{4i}^{\#}(\bar{I}_{4i}) = \begin{cases} \bar{I}_{4i} & \text{if} \quad \bar{I}_{4i} > 1 \\ \\ 1 & \text{if} \quad \bar{I}_{4i} \leq 1 \end{cases} \tag{28}$$

and set the (continuous) stress contribution with compressed fibers excluded as

$$\bar{\boldsymbol{S}}_{fi}(\bar{I}_{4i}^{\#}) = 2k_1(\bar{I}_{4i}^{\#} - 1)\exp\left(k_2(\bar{I}_{4i}^{\#} - 1)^2\right)\boldsymbol{a}_{0i} \otimes \boldsymbol{a}_{0i} = 2\mathcal{W}_f'(\bar{I}_{4i}^{\#} - 1)\boldsymbol{a}_{0i} \otimes \boldsymbol{a}_{0i} \tag{29}$$

That way

$$\bar{\boldsymbol{S}}_{fi}\left(\bar{I}_{4i}^{\#}(\bar{I}_{4i} \leq 1)\right) = \bar{\boldsymbol{S}}_{fi}(\bar{I}_{4i}^{\#} = 1) = \boldsymbol{0} \qquad \text{and} \qquad \bar{\boldsymbol{S}}_{fi}\left(\bar{I}_{4i}^{\#}(\bar{I}_{4i} \to 1^+)\right) = \bar{\boldsymbol{S}}_{fi}(\bar{I}_{4i}^{\#} \to 1^+) = \boldsymbol{0} \tag{30}$$

In other words, the stress response of the ith (aligned) fiber family when the fiber in direction $\boldsymbol{a}_{0i}$ is in compression ($\bar{I}_{4i} < 1$) is coincident to the stress response when the fiber in direction $\boldsymbol{a}_{0i}$ is unstrained ($\bar{I}_{4i} = 1$) and also coincident to the stress response in the limit $\bar{I}_{4i} \to 1^+$.

The stress contribution of the ith dispersed fiber family is given in Eq. (8) as

$$\bar{\boldsymbol{S}}_{fi}(\bar{E}_i) = 2k_1\bar{E}_i\exp\left(k_2\bar{E}_i^2\right)\left(\kappa\boldsymbol{I} + (1 - 3\kappa)\,\boldsymbol{a}_{0i} \otimes \boldsymbol{a}_{0i}\right) = 2\mathcal{W}_f'(\bar{E}_i)\boldsymbol{H}_i \tag{31}$$

with $\bar{E}_i$ given by Eq. (6). Hence, we can define a (continuous) piecewise function of the structure invariant $\bar{E}_i$ as

$$\bar{E}_i^{\star}(\bar{E}_i) = \begin{cases} \bar{E}_i & \text{if} \quad \bar{E}_i > 0 \\ \\ 0 & \text{if} \quad \bar{E}_i \leq 0 \end{cases} \tag{32}$$

and set the (continuous) stress contribution of the ith dispersed fiber family, based on the tension-compression switch $\bar{E}_i \leq 0$, as

$$\bar{\boldsymbol{S}}_{fi}(\bar{E}_i^\star) = 2k_1\bar{E}_i^\star \exp\left(k_2(\bar{E}_i^\star)^2\right)(\kappa \boldsymbol{I} + (1-3\kappa)\,\boldsymbol{a}_{0i}\otimes\boldsymbol{a}_{0i}) = 2\mathcal{W}_f'(\bar{E}_i^\star)\boldsymbol{H}_i \tag{33}$$

That way

$$\bar{\boldsymbol{S}}_{fi}\left(\bar{E}_i^\star(\bar{E}_i \leq 0)\right) = \bar{\boldsymbol{S}}_{fi}(\bar{E}_i^\star = 0) = \boldsymbol{0} \qquad \text{and} \qquad \bar{\boldsymbol{S}}_{fi}\left(\bar{E}_i^\star(\bar{E}_i \to 0^+)\right) = \bar{\boldsymbol{S}}_{fi}(\bar{E}_i^\star \to 0^+) = \boldsymbol{0} \tag{34}$$

In other words, the stress response of the ith fiber family when that fiber family is in compression in average ($\bar{E}_i < 0$) is coincident to the stress response when that fiber family is unstrained in average ($\bar{E}_i = 0$) and also coincident to the stress response in the limit $\bar{E}_i \to 0^+$. Clearly, the switch criterion defined by Eqs. (32) and (33), which is *continuous* for stresses, represents the generalization of the tension-compression switch of the aligned fiber model, i.e. Eqs. (28) and (29), to the angular dispersion model using the switch $\bar{E}_i \leq 0$ –note that they are coincident for $\kappa = 0$. This switch criterion is the one implemented in the Finite Element Analysis program Abaqus [36].

The (modified) fiber family strain energy function $\mathcal{W}_f(\bar{I}_1, \bar{I}_{4i})$ from which the stress tensor given in Eq. (33) derives is represented in Figure 8 for $\kappa = 0.226$. This three-dimensional surface is a continuous function of class C^1 at the points $(\bar{I}_1 \geq 3, \bar{I}_{4i} \leq 1) = (\bar{I}_1, 1-\kappa(\bar{I}_1-3)/(1-3\kappa))$ over the straight line associated with the value $\bar{E}_i = 0$.

According to Holzapfel and Ogden [38], this computationally advantageous tension-compression switch criterion presents a theoretical disadvantage. In that Reference it is shown that there may exist deformation states for which the fiber family is extended in average (i.e. $\bar{E}_i > 0$), but the fiber in the corresponding main orientation is under compression (i.e. $\bar{I}_{4i} < 1$). This fact becomes apparent in Figure 8 because $\bar{E}_i > 0$ at the right-hand side of the line $\bar{E}_i = 0$. Holzapfel and Ogden conclude in Ref. [38] that the correct switch, specialized herein to the purely incompressible case, is $\bar{I}_{4i} \leq 1$ and not $\bar{E}_i \leq 0$. However, note that the average contribution is always in tension when the fiber family is stretched in average, i.e. $\mathcal{W}_f'(\bar{E}_i > 0) > 0$, even if $\bar{I}_{4i} \leq 1$. We can obtain more insight on this issue from Figure 8. We observe in that Figure (green line) that the fiber family strain energy vanishes for the set of deformation states $(\bar{I}_1 > 3, \bar{I}_{4i} < 1) = (\bar{I}_1, 1-\kappa(\bar{I}_1-3)/(1-3\kappa))$ defined by $\bar{E}_i = 0$, which may be (a priori) justified by the fact that the fiber family is unstrained in average. However, if both $\bar{E}_i = 0$ and some fiber orientations are in compression (in particular $\bar{I}_{4i} < 1$), then there should be some other fiber orientations that are in tension. Arguably, we conclude that it should be $\mathcal{W}_f(\bar{E}_i = 0; \bar{I}_{4i} < 1) > 0$ in averaged terms and not $\mathcal{W}_f(\bar{E}_i = 0; \bar{I}_{4i} < 1) = 0$.

Uniaxial testing

We have also arrived to the same conclusion as that pointed out in Ref. [38] in the uniaxial test in the circumferential direction presented in Section 3. In that case, see Figure 3, we obtained deformation states for which $\bar{I}_4 < 1$ and $\bar{E} > 0$. In fact, the switch point $\bar{E} = 0$ is never attained in the cases being analyzed. The response of both arterial wall specimens when this switch is considered is the same as the one shown in Figures 3 and 4.

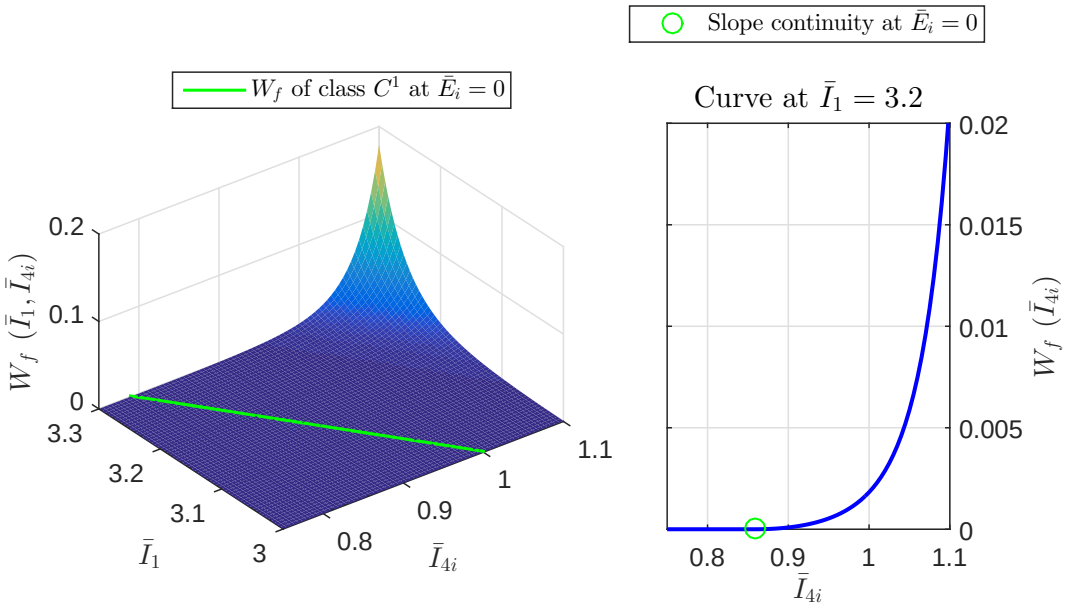

Figure 8: Strain energy function of the ith fiber family $\mathcal{W}_f\left(\bar{E}_i^\star(\bar{E}_i)\right) = \mathcal{W}_f(\bar{I}_1, \bar{I}_{4i})$ [MJ / m^3] modified according to the switch $\bar{E}_i \leq 0$ implemented in Abaqus [36]. Equations (1) and (32) are used with $k_1 = 996.6\,\text{kPa}$, $k_2 = 524.6$ and $\kappa = 0.226$.

6 A *GST*-based pre-integrated proposal which distinguishes compression from tension in fiber families and gives continuous stress functions

We have shown in Section 4 that the direct suppression of the pseudo-invariant $\bar{I}_{4i}$ in both the structure invariant $\bar{E}_i$ and the strain energy function $\mathcal{W}_f(\bar{E}_i)$ when $\bar{I}_{4i} \leq 1$ causes discontinuities in the behavior and may lead to undesirable situations where equilibrium solutions may not be found. Hence, the formulation of Section 4 requires some modifications in order to exclude individual fibers which are under compression. The recent modified fiber distribution models presented in Refs. [38] and [33] have some similarities to the structural model of Lanir [25], hence nullifying the main computational advantage of the continuum-based *GST* approaches.

In this section we propose an enhanced invariant-based continuum formulation that circumvents the difficulties that have been pointed out in the preceding sections. The present proposal is based on the definition of a new, more elaborated, generalized structure invariant which is both pre-integrated within the whole range of deformations and smooth, i.e. it yields continuous stresses. We provide closed-form expressions for the weighted invariant and the associated Generalized Structure Tensors. The resulting formulation preserves the computational advantage of the *GST* approach and is valid for any strain energy function used to model fiber dispersion. As a main novelty with respect to previous *GST* models, the present formulation predicts an additional tension-compression switch to that of $\bar{I}_{4i} \leq 1$. This additional switch will be active when the fibers in the transverse plane to the main direction $\boldsymbol{a}_{0i}$ are in compression in average and the fiber in direction $\boldsymbol{a}_{0i}$ is in extension.

As aforementioned, the structure invariant $\bar{E}_i$ represents an averaged Green–Lagrange strain measure computed over the fiber distribution associated with the ith fiber family by means of the normalized expression

$$\bar{E}_i = \frac{1}{4\pi} \int_{\Sigma} \rho\left(\theta,\varphi\right) \left[\lambda^2\left(\theta,\varphi\right) - 1\right] d\Sigma \tag{35}$$

where Σ is the surface of the unit sphere, $\theta \in [0,\pi]$ and $\varphi \in [0,2\pi]$ are spherical angles, $\lambda\left(\theta,\varphi\right)$ is the stretch of a given fiber within the distribution and $\rho\left(\theta,\varphi\right)$ is an orientation density function normalized through

$$1 = \frac{1}{4\pi} \int_{\Sigma} \rho\left(\theta,\varphi\right) d\Sigma \tag{36}$$

When we specialize the preceding expressions to a transversely isotropic fiber distribution, they read

$$\bar{E}_i = \frac{1}{4\pi} \int_{\Sigma} \rho\left(\theta\right) \left[\lambda^2\left(\theta,\varphi\right) - 1\right] d\Sigma \tag{37}$$

and

$$1 = \frac{1}{2} \int_0^{\pi} \rho\left(\theta\right) \sin\theta d\theta = \int_0^{\pi/2} \rho\left(\theta\right) \sin\theta d\theta \tag{38}$$

where the symmetry of $\rho\left(\theta\right)$ with respect to $\theta = \pi/2$ (normal plane to $\boldsymbol{a}_{0i}$) has been used. The squared stretch $\lambda^2\left(\theta,\varphi\right)$ of the fiber oriented about the material direction $\boldsymbol{N}\left(\theta,\varphi\right)$ is obtained from the isochoric Cauchy–Green deformation tensor through $\lambda^2 = \bar{\boldsymbol{C}} : \boldsymbol{N} \otimes \boldsymbol{N}$. For an arbitrary deformation tensor $\bar{\boldsymbol{C}}$, the integral of Eq. (37) yields Eq. (6), where the dispersion parameter is defined by means of

$$\kappa = \frac{1}{2} \int_0^{\pi/2} \rho\left(\theta\right) \sin^3\theta d\theta \tag{39}$$

Consider now the *mean* squared stretch $\lambda_{\pi i}^2$ of the fibers within the transverse plane to the main fiber orientation $\boldsymbol{a}_{0i}$, say π_{0i}, i.e.

$$\bar{I}_1 = \lambda_{ai}^2 + \lambda_{\pi i}^2 + \lambda_{\pi i}^2 = \bar{I}_{4i} + 2\lambda_{\pi i}^2 \quad \Rightarrow \quad \lambda_{\pi i}^2 = \frac{\bar{I}_1 - \bar{I}_{4i}}{2} > 0 \tag{40}$$

which depends on $\bar{I}_1$ and $\bar{I}_{4i}$ only and has a clear geometrical interpretation. The structure invariant $\bar{E}_i$ of Eq. (6) can be rephrased in terms of the invariants $\lambda_{\pi i}^2$ and λ_{ai}^2 as

$$\bar{E}_i = 2\kappa\lambda_{\pi i}^2 + (1-2\kappa)\,\lambda_{ai}^2 - 1 =: \bar{\lambda}_i^2 - 1 \tag{41}$$

where the invariant $\bar{\lambda}_i^2$ is the average squared stretch of the ith fiber distribution. Then, we can define a fiber angle material parameter θ_κ, which relates to the dispersion material parameter by means of $\sin^2\theta_\kappa := 2\kappa$, so the average invariant $\bar{\lambda}_i^2$ present in Eq. (41) may be interpreted as the equivalent squared stretch of the characteristic fibers in the material-dependent direction θ_κ, i.e.

$$\bar{\lambda}_i^2 = \lambda_{\pi i}^2 \sin^2\theta_\kappa + \lambda_{ai}^2 \cos^2\theta_\kappa \tag{42}$$

For $\kappa = 0$, then $\theta_\kappa = 0$ and $\bar{\lambda}_i^2 = \lambda_{ai}^2 = \bar{I}_{4i}$. For $\kappa = 1/3$, then $\theta_\kappa = \arcsin(\sqrt{2/3})$ and $\bar{\lambda}_i^2 = \frac{2}{3}\lambda_{\pi i}^2 + \frac{1}{3}\lambda_{ai}^2 = \frac{1}{3}\bar{I}_1$. For $\kappa = 1/2$, then $\theta_\kappa = \pi/2$ and $\bar{\lambda}_i^2 = \lambda_{\pi i}^2 = \frac{1}{2}(\bar{I}_1 - \bar{I}_{4i})$. On the other side, the consideration of the integrals of Eqs. (38) and (39) in Eq. (41) gives

$$\begin{aligned}\bar{E}_i &= \overbrace{\left(\int_0^{\pi/2} \rho(\theta)\sin^3\theta d\theta\right)}^{2\kappa=\sin^2\theta_\kappa}\lambda_{\pi i}^2 + \overbrace{\left(\int_0^{\pi/2}\rho(\theta)\sin\theta d\theta - \int_0^{\pi/2}\rho(\theta)\sin^3\theta d\theta\right)}^{1-2\kappa=1-\sin^2\theta_\kappa=\cos^2\theta_\kappa}\lambda_{ai}^2 - \overbrace{\int_0^{\pi/2}\rho(\theta)\sin\theta d\theta}^{1} \\ &= \int_0^{\pi/2}\rho(\theta)\left[\lambda_{\pi i}^2\sin^2\theta + \lambda_{ai}^2\cos^2\theta - 1\right]\sin\theta d\theta \end{aligned} \tag{43}$$

Since $\lambda_{\pi i}^2$ represents the average of the squared fiber stretches within the plane π_{0i} and, obviously, λ_{ai}^2 is the average of the squared fiber stretch(es) in direction $\boldsymbol{a}_{0i}$, then we recognize the average of the squared fiber stretches for a given angle $\theta \in [0, \pi/2]$, over the domain $\varphi \in [0, 2\pi]$, as

$$\lambda_{aver}^2(\theta) = \lambda_{\pi i}^2\sin^2\theta + \lambda_{ai}^2\cos^2\theta \tag{44}$$

whereupon Eq. (43) reads —compare to Eq. (37)

$$\bar{E}_i = \int_0^{\pi/2}\rho(\theta)\left[\lambda_{aver}^2(\theta) - 1\right]\sin\theta d\theta \tag{45}$$

That is, although the ith fiber family does not obey a transversely isotropic deformation pattern in general, we can compute the structure invariant $\bar{E}_i$ by means of the integration of an equivalent transversely isotropic deformation pattern for which the main fiber is stretched through $\lambda_{ai}^2 = \bar{I}_{4i}$ and the transverse plane is (evenly) stretched by means of $\lambda_{\pi i}^2 = (\bar{I}_1 - \bar{I}_{4i})/2$, such that each fiber is stretched $\lambda_{aver}(\theta)$ as given by Eq. (44). Finally, we can obtain the Generalized Structure Tensor $\boldsymbol{H}_i$ taking the total gradient of the structure invariant $\bar{E}_i$ expressed in terms of $\bar{I}_1$ and $\bar{I}_{4i}$, i.e.

$$\boldsymbol{H}_i = \frac{d\bar{E}_i(\bar{I}_1, \bar{I}_{4i})}{d\bar{\boldsymbol{C}}} = \frac{\partial\bar{E}_i}{\partial\bar{I}_1}\frac{d\bar{I}_1}{d\bar{\boldsymbol{C}}} + \frac{\partial\bar{E}_i}{\partial\bar{I}_{4i}}\frac{d\bar{I}_{4i}}{d\bar{\boldsymbol{C}}} = \kappa\boldsymbol{I} + (1-3\kappa)\boldsymbol{a}_{0i}\otimes\boldsymbol{a}_{0i} \tag{46}$$

We have just seen that for each arbitrary isochoric deformation and distributed fiber family we can define an equivalent transversely isotropic deformation state defined by the main fiber squared stretch λ_{ai}^2 and the mean squared stretch in the transverse plane $\lambda_{\pi i}^2$, from which we can first compute (pre-integrate) the structure invariant $\bar{E}_i$ (through Eq. (41)) and then derive the generalized structure tensor $\boldsymbol{H}_i$ (through Eq. (46)). The structure invariant $\bar{E}_i$ and the generalized structure tensor $\boldsymbol{H}_i$ are the two only variables needed to compute the hyperelastic stresses associated with the ith fiber family, recall Eq. (8). Indeed, this is the feature that makes the *GST* approach so appealing from a numerical perspective. In what follows, above all, we try to preserve this computational advantage. Motivated by the preceding analysis, we derive a modified structure invariant $\bar{\epsilon}_i$ that pre-integrates the equivalent transversely isotropic deformation pattern excluding the respective fibers which are under compression. This enhanced approach provides continuous stresses for all ranges of deformations. Furthermore, the corresponding stresses may be obtained in closed-form using only the invariants $\bar{I}_1$ and $\bar{I}_{4i}$, hence furnishing a continuum-based *GST* formulation that is well-suited for finite element implementation.

If $\lambda_{ai}^2 \neq \lambda_{\pi i}^2$, then the squared stretch $\lambda_{aver}^2(\theta)$ given in Eq. (44) is a strictly monotonic function in terms of θ that goes from $\lambda_{aver}^2(0) = \lambda_{ai}^2$ to $\lambda_{aver}^2(\pi/2) = \lambda_{\pi i}^2$. Therefore, either if $\lambda_{ai} \leq 1$ and $\lambda_{\pi i} > 1$ or if $\lambda_{ai} > 1$ and $\lambda_{\pi i} \leq 1$, then Eq. (44) gives an angle $\Theta(\bar{I}_1, \bar{I}_{4i})$ for which $\lambda_{aver}^2(\Theta) = 1$, i.e.

$$\cos^2\Theta = \frac{\left(\bar{I}_{4i} - 1\right) - \left(\bar{I}_1 - 3\right)}{3\left(\bar{I}_{4i} - 1\right) - \left(\bar{I}_1 - 3\right)} \quad \text{or} \quad \sin^2\Theta = \frac{2\left(\bar{I}_{4i} - 1\right)}{3\left(\bar{I}_{4i} - 1\right) - \left(\bar{I}_1 - 3\right)} \tag{47}$$

Consider first the case for which $\lambda_{ai} \leq 1$ and $\lambda_{\pi i} > 1$, i.e. the main fiber is unstrained or in compression and the fibers in the transverse plane are stretched in average. This occurs when $\bar{I}_{4i} \leq 1$ and $\bar{I}_1 \geq 3$ (note that $\bar{I}_1 \not< 3$ for purely incompressible materials), which define the first tension-compression switch of the present formulation. Then the fibers are shortened for $0 \leq \theta < \Theta$, unstrained for $\theta = \Theta$ and stretched for $\Theta < \theta \leq \pi/2$, see the corresponding region in Figure 9. We assume that only the fibers which are under extension contribute to the modified structure invariant $\bar{\epsilon}_i$. Hence, if $\bar{I}_{4i} \leq 1$ and $\bar{I}_1 \geq 3$, $\bar{\epsilon}_i$ is given by

$$\bar{\epsilon}_i = \int_{\Theta}^{\pi/2} \rho(\theta)\left[\lambda_{aver}^2(\theta) - 1\right]\sin\theta d\theta \tag{48}$$

$$= \left(\frac{1}{2}\int_{\Theta}^{\pi/2} \rho(\theta)\sin^3\theta d\theta\right)\bar{I}_1 + \left(\int_{\Theta}^{\pi/2} \rho(\theta)\sin\theta d\theta - \frac{3}{2}\int_{\Theta}^{\pi/2} \rho(\theta)\sin^3\theta d\theta\right)\bar{I}_{4i} - \int_{\Theta}^{\pi/2} \rho(\theta)\sin\theta d\theta \tag{49}$$

$$= \varkappa_1(\Theta)(\bar{I}_1 - 3) + \left[\iota_1(\Theta) - 3\varkappa_1(\Theta)\right](\bar{I}_{4i} - 1) \tag{50}$$

where we have defined the first modified unit function ι_1 and the first modified dispersion parameter $\varkappa_1$, both depending on the angle $\Theta(\bar{I}_1, \bar{I}_{4i})$, as

$$\iota_1(\Theta) = \int_{\Theta}^{\pi/2} \rho(\theta)\sin\theta d\theta \tag{51}$$

and

$$\varkappa_1(\Theta) = \frac{1}{2}\int_{\Theta}^{\pi/2} \rho(\theta)\sin^3\theta d\theta \tag{52}$$

In the limit $\Theta \to 0^+$, then $\iota_1(0^+) \to 1$ and $\varkappa_1(0^+) \to \kappa$, cf. Eqs. (38) and (39), so $\bar{\epsilon}_i(0^+) \to \bar{E}_i$. Equations (51) and (52) are valid for any normalized orientation density function $\rho(\theta)$. When they

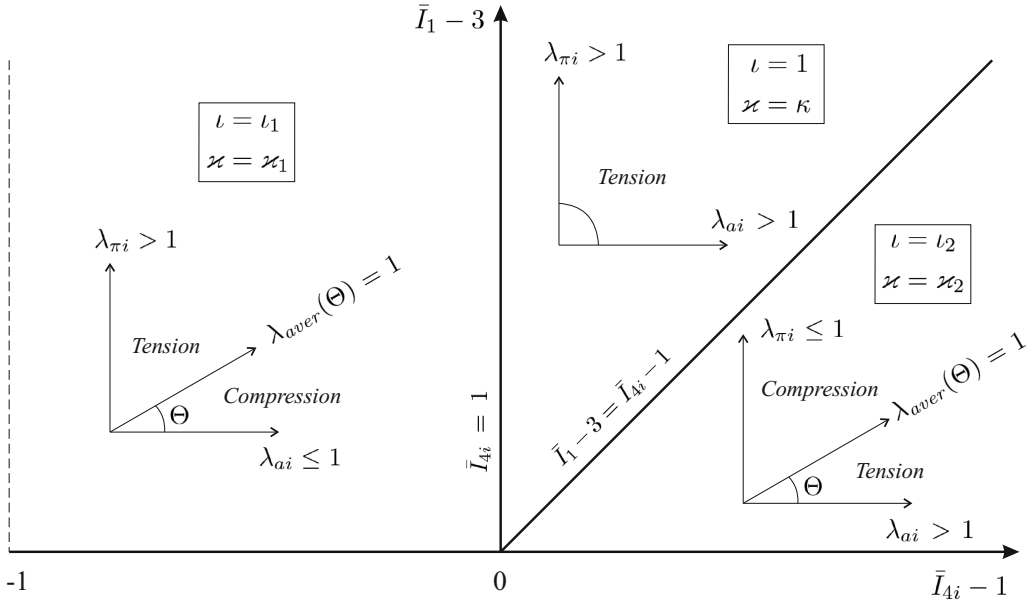

Figure 9: Schematic behavior of the ith distribution of fibers and definition of ι and $\varkappa$ for each region of the plane $\{\bar{I}_1 - 3, \bar{I}_{4i} - 1\}$ under study. The modified structure invariant is given by $\bar{\epsilon}_i = \varkappa(\bar{I}_1 - 3) + (\iota - 3\varkappa)(\bar{I}_{4i} - 1)$. The associated modified Generalized Structure Tensor is given by $\boldsymbol{H}_i^{mod} = \varkappa \boldsymbol{I} + (\iota - 3\varkappa)\boldsymbol{a}_{0i} \otimes \boldsymbol{a}_{0i}$.

are specialized to the standard π-periodic von Mises distribution of the form

$$\rho\left(\theta\right) = 2\sqrt{\frac{2b}{\pi}} \frac{1}{\operatorname{erfi}\left(\sqrt{2b}\right)} \exp(2b\cos^2\theta) \tag{53}$$

where $b > 0$ is the concentration parameter (related to κ through Eq. (39)) and $\operatorname{erfi}(x) = -i\operatorname{erf}(ix)$ is the imaginary error function, then Eqs. (51) and (52) are given in closed-form in terms of $\Theta(\bar{I}_1, \bar{I}_{4i})$ through

$$\iota_1(\Theta) = \frac{\operatorname{erfi}\left(\sqrt{2b}\cos\Theta\right)}{\operatorname{erfi}\left(\sqrt{2b}\right)} \tag{54}$$

and

$$\varkappa_1(\Theta) = \left(\frac{1}{2} + \frac{1}{8b}\right) \frac{\operatorname{erfi}\left(\sqrt{2b}\cos\Theta\right)}{\operatorname{erfi}\left(\sqrt{2b}\right)} - \frac{1}{2}\sqrt{\frac{1}{2b\pi}} \frac{\cos\Theta \exp(2b\cos^2\Theta)}{\operatorname{erfi}\left(\sqrt{2b}\right)} \tag{55}$$

Note that $\iota_1(0) = 1$ and $\varkappa_1(0) = \kappa$ [30].

Consider now the case for which $\lambda_{ai} > 1$ and $\lambda_{\pi i} \leq 1$, i.e. the main fiber is stretched and the fibers in the transverse plane are unstrained or in compression in average. This occurs when $\bar{I}_{4i} > 1$ and $\bar{I}_1 - 3 \leq \bar{I}_{4i} - 1$, which define the second tension-compression switch of the present

formulation. Then the fibers are stretched for $0 \leq \theta < \Theta$, unstrained for $\theta = \Theta$ and shortened for $\Theta < \theta \leq \pi/2$, see the corresponding region in Figure 9. Thus, if $\bar{I}_{4i} > 1$ and $\bar{I}_1 - 3 \leq \bar{I}_{4i} - 1$, the modified structure invariant $\bar{\epsilon}_i$ is

$$\bar{\epsilon}_i = \int_0^{\Theta} \rho\left(\theta\right) \left[\lambda^2_{aver}\left(\theta\right) - 1\right] \sin\theta d\theta \tag{56}$$

$$= \int_0^{\pi/2} \rho\left(\theta\right) \left[\lambda^2_{aver}\left(\theta\right) - 1\right] \sin\theta d\theta - \int_{\Theta}^{\pi/2} \rho\left(\theta\right) \left[\lambda^2_{aver}\left(\theta\right) - 1\right] \sin\theta d\theta \tag{57}$$

$$= \varkappa_2(\Theta)(\bar{I}_1 - 3) + \left[\iota_2(\Theta) - 3\varkappa_2(\Theta)\right](\bar{I}_{4i} - 1) \tag{58}$$

where Eqs. (38), (39), (51) and (52) have been used and ι_2 and $\varkappa_2$ are the second unit function and second modified dispersion parameter which remarkably take the values

$$\iota_2(\Theta) = 1 - \iota_1(\Theta) \tag{59}$$

$$\varkappa_2(\Theta) = \kappa - \varkappa_1(\Theta) \tag{60}$$

In this case, the limit $\Theta \to \frac{\pi}{2}^-$ yields $\iota_2(\frac{\pi}{2}^-) = 1 - \iota_1(\frac{\pi}{2}^-) \to 1 - 0 = 1$ and $\varkappa_2(\frac{\pi}{2}^-) = \kappa - \varkappa_1(\frac{\pi}{2}^-) \to \kappa - 0 = \kappa$, so $\bar{\epsilon}_i(\frac{\pi}{2}^-) \to \bar{E}_i$.

Finally, if $\lambda_{ai} > 1$ and $\lambda_{\pi i} > 1$, then all the fibers under the modified deformation state are stretched, so there is no angle $0 \leq \Theta \leq \pi/2$ for which $\lambda_{aver}(\Theta) = 1$. The integrals to be used in this case are those given in Eqs. (38), (39), so $\bar{\epsilon}_i = \bar{E}_i$ in this case. This occurs when $\bar{I}_{4i} > 1$ and $\bar{I}_1 - 3 > \bar{I}_{4i} - 1$, see Figure 9. The case for which all the fibers under the modified deformation state are in compression is not possible for purely isochoric materials because this case requires that $\bar{I}_1 < 3$. In Figure 9 we show the different regions in the plane $\{\bar{I}_1, \bar{I}_{4i}\}$ where the different expressions of the modified unit functions ι and dispersion parameters $\varkappa$ apply. Two tension-compression switch lines are clearly distinguished.

As a summary, we propose the use of the modified invariant

$$\bar{\epsilon}_i = \varkappa(\bar{I}_1 - 3) + (\iota - 3\varkappa)(\bar{I}_{4i} - 1) \tag{61}$$

which is to be assessed taking into consideration two tension-compression switches, the first one being characterized by the compression of the main fiber orientation $\boldsymbol{a}_{0i}$ and the second one characterized by the average compression of the fibers within the referential plane π_{0i} normal to $\boldsymbol{a}_{0i}$

$$\bar{\epsilon}_i(\bar{I}_1, \bar{I}_{4i}) = \begin{cases} \varkappa_1(\bar{I}_1 - 3) + (\iota_1 - 3\varkappa_1)(\bar{I}_{4i} - 1) & \text{if} \quad \bar{I}_{4i} \leq 1 \\ \varkappa_2(\bar{I}_1 - 3) + (\iota_2 - 3\varkappa_2)(\bar{I}_{4i} - 1) & \text{if} \quad \bar{I}_{4i} > 1 \quad \text{and} \quad \bar{I}_1 - 3 \leq \bar{I}_{4i} - 1 \\ \kappa(\bar{I}_1 - 3) + (1 - 3\kappa)(\bar{I}_{4i} - 1) & \text{if} \quad \bar{I}_{4i} > 1 \quad \text{and} \quad \bar{I}_1 - 3 > \bar{I}_{4i} - 1 \end{cases} \tag{62}$$

where Eqs. (39), (51), (52), (59) and (60), along with the angle of Eq. (47), are to be used. At least for the special case of the standard π-periodic von Mises distribution of Eq. (53), the expressions given in Eqs. (54) and (55) permit the computation of the invariant $\bar{\epsilon}(\bar{I}_1, \bar{I}_{4i})$ in closed-form.

We can obtain the expression of the modified Generalized Structure Tensor differentiating the modified structure tensor $\bar{\epsilon}_i$ of Eq. (62) through

$$\boldsymbol{H}_i^{mod} = \frac{d\bar{\epsilon}_i(\bar{I}_1, \bar{I}_{4i})}{d\bar{\boldsymbol{C}}} = \frac{\partial\bar{\epsilon}_i}{\partial\bar{I}_1}\frac{d\bar{I}_1}{d\bar{\boldsymbol{C}}} + \frac{\partial\bar{\epsilon}_i}{\partial\bar{I}_{4i}}\frac{d\bar{I}_{4i}}{d\bar{\boldsymbol{C}}} = \varkappa\boldsymbol{I} + (\iota - 3\varkappa)\boldsymbol{a}_0 \otimes \boldsymbol{a}_0 \tag{63}$$

where the modified parameters $\varkappa$ and ι are specified in Eq. (62) and Figure 9. In the partial derivatives present in Eq. (63) it has been taken into account that $\varkappa_1$ and ι_1 depend on the deformation state through the invariants $\bar{I}_1$ and $\bar{I}_{4i}$, recall Eqs. (51) and (52), along with (47). However, these partial derivatives cancel to each other and the final expression of $\boldsymbol{H}_i^{mod}$ results as simple as in Eq. (63). Again, Eqs. (54) and (55) allow the computation of $\boldsymbol{H}_i^{mod}$ in closed-form for each deformation state of the continuum.

The fiber family strain energy function of Eq. (1) is then expressed in terms of the modified structure tensor $\bar{\epsilon}_i$ of Eq. (62) as

$$\mathcal{W}_f(\bar{\epsilon}_i) = \frac{k_1}{2k_2}\left[\exp\left(k_2\bar{\epsilon}_i^2\right) - 1\right] \tag{64}$$

The stress contribution of the ith dispersed fiber family given in Eq. (8) results into

$$\bar{\boldsymbol{S}}_{fi} = 2\frac{d\mathcal{W}_f(\bar{\epsilon}_i)}{d\bar{\boldsymbol{C}}} = 2\frac{d\mathcal{W}_f(\bar{\epsilon}_i)}{d\bar{\epsilon}_i}\frac{d\bar{\epsilon}_i}{d\bar{\boldsymbol{C}}} = 2\mathcal{W}_f'(\bar{\epsilon}_i)\boldsymbol{H}_i^{mod} \tag{65}$$

As a main difference with the stresses predicted by the model based on the structure invariant $\bar{E}_i$ and the switch $\bar{I}_{4i} \leq 1$ of Section 4, we note that this modified approach gives continuous stresses for all the ranges of deformation. This is due to the fact that the modified Generalized Structure Tensor $\boldsymbol{H}_i^{mod}$ given in Eq. (63) is continuous along the first switch line, defined by $\bar{I}_{4i} = 1$ (where $\Theta = 0$, so $\iota_1(0) = 1$ and $\varkappa_1(0) = \kappa$), and also over the second switch line, defined by $\bar{I}_1 - 3 = \bar{I}_{4i} - 1$ (where $\Theta = \pi/2$, so $\iota_2(\pi/2) = 1$ and $\varkappa_2(\pi/2) = \kappa$). In this case, both switches are activated in a continuous way. We also note that the stress tensor $\bar{\boldsymbol{S}}_{fi}$ contains an anisotropic contribution in $\boldsymbol{H}_i^{mod}$ even though the switches are activated.

The fiber family strain energy function $\mathcal{W}_f(\bar{\epsilon}_i)$, with $\bar{\epsilon}_i$ given in Eq. (62), is represented in Figure 10 using the material constants of Section 4. The strain energy function of Figure 10 is of class C^1 over the switch lines $(\bar{I}_1, \bar{I}_{4i} = 1)$ and $(\bar{I}_1, \bar{I}_{4i} = \bar{I}_1 - 2)$.

When the strain energy function shown in Figure 10 is compared to the strain energy function shown in Figure 8 (used in Abaqus), we can also observe that the former one has a single minimum at the undeformed configuration $(\bar{I}_1 = 3, \bar{I}_{4i} = 1)$, whereas the latter one presents the same minimum value all along the line $\bar{E}_i = 0$ (and also for $\bar{E}_i < 0$ if the switch of that section is considered) which, as aforementioned, seems to be a physically unrealistic situation. The present enhanced formulation circumvents that issue as well.

Uniaxial testing

We show in Figure 11 the results of the uniaxial tensile test about the circumferential direction (see Figure 1) obtained using the present modified structure invariant $\bar{\epsilon}$. The equations to be solved in this case are Eqs. (14) and (15), but substituting $\bar{E}$ by $\bar{\epsilon}$, κ by $\varkappa$ and $(1-3\kappa)$ by $(\iota-3\varkappa)$. We observe that the response is continuous and that the interval for which $\bar{I}_4 \leq 1$ is preserved with respect to the case with fibers bearing compression, see Figure 3. That is, abrupt changes from $\bar{I}_4 \leq 1$ to $\bar{I}_4 > 1$ are prevented because the modified invariant $\bar{\epsilon}$ is smooth enough. Interestingly, deformation states for which $\bar{I}_4 > 1$ and $\bar{I}_1 - 3 \leq \bar{I}_4 - 1$ (second tension-compression switch introduced above) also occur during this calculation, more specifically at $\lambda_1 \approx 1$.

Remark We want to emphasize the differences between the present approach and the formulation recently proposed by Holzapfel and Ogden in Reference [38]. The present procedure represents an

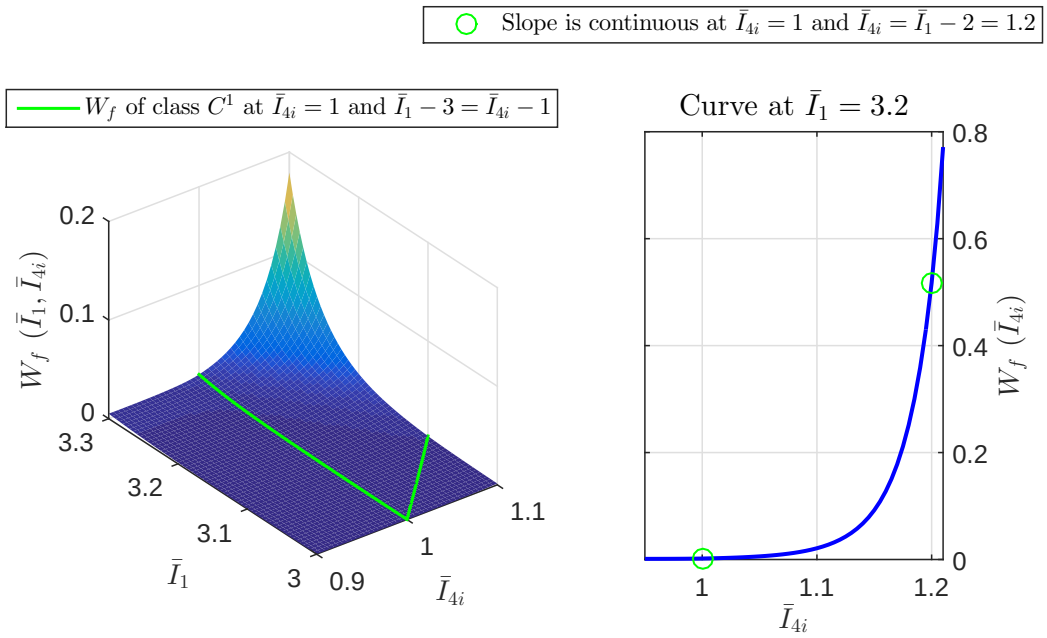

Figure 10: Strain energy function of the ith fiber family $\mathcal{W}_f(\bar{\epsilon}_i) = \mathcal{W}_f(\bar{I}_1, \bar{I}_{4i})$ [MJ / m^3] based on the switches given in Eq. (62). The material parameters are $k_1 = 996.6\,\text{kPa}$, $k_2 = 524.6$ and $\kappa = 0.226$ ($b = 1.084$).

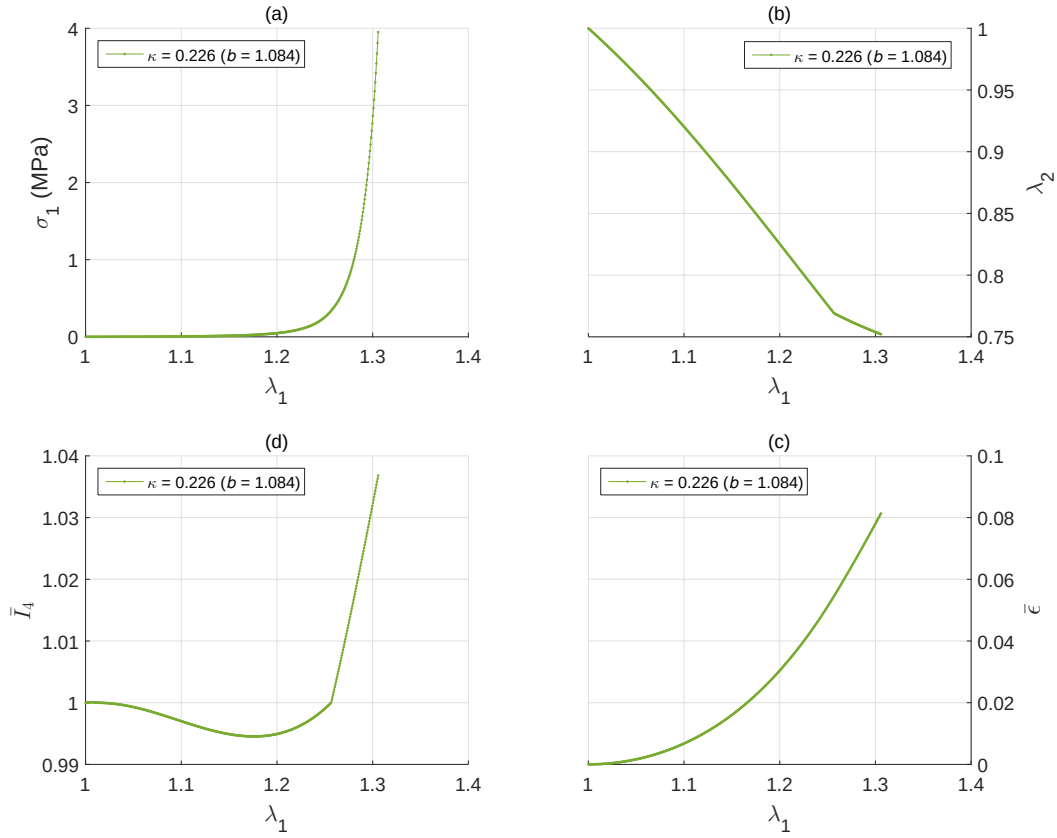

Figure 11: Uniaxial test over the circumferential specimen (direction 1 in Figure 1) using the modified formulation of Section 6 based on two different switches. Clockwise from left-up corner: (a) Uniaxial stress in circumferential direction σ_1 (b) Transverse stretch in axial direction λ_2 (c) Structure invariant $\bar{\epsilon} = \varkappa(\bar{I}_1 - 3) + (\iota - 3\varkappa)(\bar{I}_4 - 1)$ (d) Pseudo-invariant $\bar{I}_4$: squared stretch of the fibres in the main orientations $\boldsymbol{a}_{0i}$.

invariant-based continuum approach which follows the essence of the *GOH* model of Ref. [4], also similar in nature to that of the previous work of Ref. [31]. On the other hand, the proposal of Ref. [38] represents a distributed fiber model which follows in essence the ideas of the structural model of Lanir [25]. Our proposal is a Generalized Structure Tensor approach based on any fiber family strain energy function $\mathcal{W}_f(\bar{\epsilon}_i)$, the pre-integrated invariant of Eq. (61), the invariant-based switches specified in Eq. (62), the *GST* of Eq. (63) and the associated stresses given in Eq. (65), where note that $\mathcal{W}'_f(\bar{\epsilon}_i)$ can be freely selected without modifying any of the previous pre-integrated expressions. The proposal of Holzapfel and Ogden in Ref. [38] is an Angular Integration approach based on the fiber family strain energy function of Eq. (91) of Ref. [38], the relation between the critical angles $\Phi\,(\Theta)$ obtained from the solution of the non-linear Equation (113) of Ref. [38], the associated stresses given in Eqs. (92)–(94) of Ref. [38] and the doble integral coefficients of Eqs. (95)–(100) of Ref. [38], which note, are to be integrated numerically on the unit sphere taking into account the deformation-dependent critical angles associated with each integration point of the finite element mesh. Note that Eqs. (103) to (109) of Ref. [38] are obtained for the simple energy given by Eq. (76) of the same reference, which is not that of the *GOH* model. Even though Angular Integration procedures are better in the sense that they give more accurate results in general [40], the present formulation is better in the sense that it fully preserves the *GST* philosophy and is more expedient and efficient for finite element analysis, which is probably the main reason for the use of the less accurate pre-integrated *GST* models.

7 Conclusions

The Gasser-Ogden-Holzapfel model is considered one of the milestones in the analysis of soft biological tissues when considering the fiber distribution, orientation and dispersion. In order to arrive at an efficient model for finite element simulation, fiber distribution, orientation and dispersion are considered through Generalized Structure Tensors. It is usually assumed that fibers in compression do not contribute to the overall stiffness. Since in this model the contribution of fiber families are pre-integrated and encapsulated in the Generalized Structure Tensor and structure invariant, a tension-compression switch for each fiber family is usually employed. We have shown that some choices for this switch have a strong influence on the behavior in the range of interest and may also produce unphysical discontinuities in the stress-strain behavior.

In this paper we have analyzed different proposals regarding their physical implications and proposed an alternative. With our proposal we analyze which part of the fiber distribution is working in compression, determining the critical angle at which fibers are unstretched in average terms. The procedure naturally results in two distinct switches. Modified structure tensors and parameters are given as a function of the usual set of invariants so the appealing pre-integration approach is still preserved regardless of the strain energy function employed for the fibers.

However, for isotropic, transversely isotropic or orthotropic materials, if the purpose is to perform finite element simulations using the composite material as a whole rather than to perform an analysis employing information from the material constituents, we prefer the purely phenomenological approach [18], [10], [11]: no switch is needed, no parameter fitting procedure is employed and up to six experimental curves are exactly captured in orthotropic materials [17].

Acknowledgements

Partial financial support for this work has been given by grant DPI2011-26635 from the Dirección General de Proyectos de Investigación of the Ministerio de Economía y Competitividad of Spain.

References

[1] YC Fung (2013). Biomechanics: mechanical properties of living tissues. Springer Science & Business Media.

[2] JD Humphrey (2013). Cardiovascular solid mechanics: cells, tissues, and organs. Springer Science & Business Media.

[3] GA Holzapfel, T Gasser, RW Ogden. A new constitutive framework for arterial wall mechanics and a comparative study of material models. Journal of Elasticity, 61:1–18, 2000.

[4] T Gasser, R Ogden, GA Holzapfel. Hyperelastic modelling of arterial layers with distributed collagen fiber orientations. Journal of the Royal Society Interface, 3:13–35, 2006.

[5] PB Canham, HM Finlay, JG Dixon, DR Boughner, A Chen. Measurements from light and polarised light microscopy of human coronary arteries fixed at distending pressure. Cardiovascular Research, 23(11): 973-982. 1989.

[6] C Boote, S Hayes, M Abahussin, KM Meek. Mapping collagen organization in the human cornea: left and right eyes are structurally distinct. Investigative Ophthalmology & Visual Science, 47(3): 901-908. 2006.

[7] HM Finlay, P Whittaker, PB Canham. Collagen organization in the branching region of human brain arteries. Stroke, 29(8): 1595-1601. 1998.

[8] Y Komai, T Ushiki. The three-dimensional organization of collagen fibrils in the human cornea and sclera. Invest Ophthalmol Vis Sci, 32(8): 2244-2258. 1991.

[9] AJ Schriefl, G Zeindlinger, DM Pierce, P Regitnig, GA Holzapfel. Determination of the layer-specific distributed collagen fibre orientations in human thoracic and abdominal aortas and common iliac arteries. Journal of the Royal Society Interface, 9: 3081-3093. 2011.

[10] M Latorre, FJ Montáns. Extension of the Sussman–Bathe spline-based hyperelastic model to incompressible transversely isotropic materials. Computers & Structures, 122:13–26, 2013.

[11] M Latorre, FJ Montáns. What-You-Prescribe-Is-What-You-Get orthotropic hyperelasticity. Computational Mechanics, 53(6): 1279–1298, 2014.

[12] M Latorre, FJ Montáns. On the interpretation of the logarithmic strain tensor in an arbitrary system of representation. International Journal of Solids and Structures, 51(7):1507-1515, 2014.

[13] Z Fiala. Discussion of "On the interpretation of the logarithmic strain tensor in an arbitrary system of representation" by M Latorre and FJ Montáns. International Journal of Solids and Structures, 56–57:290–291, 2015.

[14] M Latorre, FJ Montáns. Response to Fiala's comments on "On the interpretation of the logarithmic strain tensor in an arbitrary system of representation". International Journal of Solids and Structures, 56–57, 292, 2015.

[15] JG Murphy. Evolution of anisotropy in soft tissue. Proceedings of the Royal Society of London A: Mathematical, Physical and Engineering Sciences, 2161(470): 20130548. 2014.

[16] M Latorre, FJ Montáns. Material-symmetries congruency in transversely isotropic and orthotropic hyperelastic materials. European Journal of Mechanics - A/Solids, 53:99–106, 2015.

[17] M Latorre, X Romero, FJ Montáns. The relevance of transverse deformation effects in hyperelastic, orthotropic incompressible materials and the recovery of the infinitesimal framework. Under review.

[18] T Sussman, KJ Bathe. A model of incompressible isotropic hyperelastic material behavior using spline interpolations of tension-compression test data. Communications in Numerical Methods in Engineering, 25(1):53–63, 2009.

[19] M Miñano, FJ Montáns. A new approach to modeling isotropic damage for Mullins effect in hyperelastic materials. International Journal of Solids and Structures, 67–68: 272–282. 2015

[20] M Latorre, FJ Montáns. Anisotropic finite strain viscoelasticity based on the Sidoroff multiplicative decomposition and logarithmic strains. Computational Mechanics, 56(3):503–531. 2015.

[21] M Latorre, FJ Montáns. Fully anisotropic finite strain viscoelasticity based on a reverse multiplicative decomposition and logarithmic strains. Computers and Structures. In press.

[22] AJM Spencer (1984). Constitutive theory for strongly anisotropic solids. In Continuum theory of the mechanics of fibre-reinforced composites, 1-32. Springer Vienna.

[23] GA Holzapfel (2000). Nonlinear solid mechanics. Chichester: Wiley.

[24] Y Lanir. A structural theory for the homogeneous biaxial stress-strain relationships in flat collagenous tissues. Journal of biomechanics, 12(6):423–436, 1979.

[25] Y Lanir. Constitutive equations for fibrous connective tissues. Journal of biomechanics, 16(1):1–12, 1983.

[26] MS Sacks. Incorporation of experimentally-derived fiber orientation into a structural constitutive model for planar collagenous tissues. Journal of Biomechanical Engineering, 125(2), 280-287. 2003.

[27] NJ Driessen, CV Bouten, FP Baaijens. A structural constitutive model for collagenous cardiovascular tissues incorporating the angular fiber distribution. Journal of Biomechanical Engineering, 127(3), 494-503. 2005.

[28] V Alastrué, B Calvo, E Pena, M Doblaré. Biomechanical modeling of refractive corneal surgery. Journal of biomechanical engineering, 128(1), 150-160. 2006.

[29] GA Ateshian, V Rajan, NO Chahine, CE Canal, CT Hung. Modeling the matrix of articular cartilage using a continuous fiber angular distribution predicts many observed phenomena. Journal of Biomechanical Engineering, 131(6), 061003. 2009.

[30] GA Holzapfel, JA Niestrawska, RW Ogden, AJ Reinisch, AJ Schriefl. Modelling non-symmetric collagen fiber dispersion in arterial walls. Journal of the Royal Society Interface, 12: 20150188, 2015.

[31] AD Freed, DR Einstein, I Vesely. Invariant formulation for dispersed transverse isotropy in aortic heart valves: an efficient means for modeling fiber splay. Biomechanics and Modeling in Mechanobiology, 4(2–3):100–117. 2005.

[32] A Pandolfi, M Vasta. Fiber distributed hyperelastic modeling of biological tissues. Mechanics of Materials, 44:151–162, 2012.

[33] AV Melnik, HB Da Rocha, A Goriely. On the modeling of fiber dispersion in fiber-reinforced elastic materials. International Journal of Non-Linear Mechanics, In Press, 2015.

[34] DH Cortes, DM Elliott. Accurate prediction of stress in fibers with distributed orientations using generalized high-order structure tensors. Mechanics of Materials, 75:73–83, 2014.

[35] T Shearer. A new strain energy function for the hyperelastic modelling of ligaments and tendons based on fascicle microstructure. Journal of biomechanics, 48(2), 290-297. 2015.

[36] Dassault Systemes Simulia Corp, 2013. Abaqus 6.13 Analysis User's Guide. In: Section 22.5.3: Anisotropic Hyperelastic Behavior.

[37] Adina R&D Inc. ADINA Theory and modelling guide. Adina, Watertown, 2012.

[38] GA Holzapfel, RW Ogden. On the tension-compression switch in soft fibrous solids. European Journal of Mechanics A/Solids, 49:561–569, 2015.

[39] D Li, AM Robertson. A structural multi-mechanism constitutive equation for cerebral arterial tissue. International Journal of Solids and Structures, 46:2920–2928, 2009.

[40] DH Cortes, SP Lake, JA Kadlowec, LJ Soslowsky, DM Elliott. Characterizing the mechanical contribution of fiber angular distribution in connective tissue: comparison of two modeling approaches. Biomechanics and Modeling in Mechanobiology, 9:651–658. 2010.